Renewable and Sustainable Energy Reviews 13 (2009) 1760–1780

Contents lists available at ScienceDirect

Renewable and Sustainable Energy Reviews

journal homepage: www.elsevier.com/locate/rser

Progress of mathematical modeling on ejectors

S. He, Y. Li, R.Z. Wang *

Institute of Refrigeration and Cryogenics, Shanghai Jiao Tong University, Shanghai 200240, PR China

ARTICLE INFO

Article history:
Received 22 August 2008
Accepted 30 September 2008

Keywords:
Ejector
Mathematical model
Thermodynamic model
Dynamic model

ABSTRACT

In ejector refrigeration systems, the performance of the ejector is critical to the performance, capability, size and cost of the whole system. Construction of mathematical models has been used as an effective method for analyzing the performance of the ejector as well as the whole refrigeration system. These models can also be used to guide system operation, interpret experimental results and assist in system design and optimization. The overall objective of this paper is to provide a review of various researches of the mathematical model on the hydrodynamic and thermodynamic character within the ejector. The paper first briefly describes ejector including fundamental principle, flowing and mixing mechanism and the method of model establishment. Then various models consisting of ideal assumptions, governing equations, auxiliary conditions, solution methods and main results are presented. The models can be classified into two main categories: (i) steady thermodynamic models which can be further subdivided into single-phase flow model and two-phase flow model and (ii) dynamic models which are also subdivided according to the flowing phases considered. It has been shown that the dynamic models have higher prediction precision and give more information compared with the steady thermodynamic models. In addition, the simplified empirical and semi-empirical models based on measured data are briefly discussed. This review is useful for understanding the evolution process and the current status of the mathematical models on ejector and highlighting the key aspects of model improvement such as the mixing mechanism, the capture of the shock wave, etc.

Contents

* Corresponding author. Tel.: +8621 3420 6548; fax: +8621 3420 6548.
E-mail address: rzwang@sjtu.edu.cn (R.Z. Wang).

1364-0321/$ – see front matter
doi:10.1016/j.rser.2008.09.032

Nomenclature

A	cross-section area (m^2)
c	local sonic velocity (m/s)
C_p	constant-pressure heat capacity (kJ/kg K)
D	diameter (m)
E	total energy, Eq. (121)
f	friction factor, Eqs. (42), (45), (46), (92)
h	specific enthalpy (kJ/kg)
k	turbulent kinetic energy, Eqs. (4), (124)
l	length (m), Eqs. (45), (46), (92)
M	Mach number
m	mass flow rate (kg/s)
P	pressure (MPa)
R	condensation rate, Eqs. (108), (112)
Re	Reynolds number, Eq. (42)
R_g	universal gas constant (kJ/kg K)
s	entropy (kJ/kg)
T	temperature (K)
u	velocity (m/s)
U, V, W	velocities in various directions (m/s)
x	location along the ejector axis(m), Eqs. (4), (94–96); quality of the fluid (kg/kg)
z	axial coordinate in cylindrical geometry (m)

Greek letters

ε	void fraction, Eqs. (106), (109), (110), (115), (117); rate of turbulent energy dissipation
γ	heat capacity ratio
Φ	dissipation energy (kJ/m^3 s), Eq. (136)
Γ	production rate
η	isentropic efficiency
μ	dynamic viscosity (Pa s)
ρ	density (kg/m^3)
τ	shear stress
υ	specific volume (m^3/kg)
Ω	area contraction ratio
ω	mass flow ratio
ξ	momentum loss factor, Eq. (92)

Subscripts

c	condenser
d	diffuser
e	exit; evaporator
f	saturated liquid, Eqs. (32) and (33)
g	generator; saturated vapor, Eqs. (32), (33); gas phase
i	inlet, location along ejector axis
is	isentropic process, Eqs. (43), (44)
l	liquid phase
lg	phase change
m	mixture; mixing section
n	primary nozzle
nt	nozzle throat
p	primary stream
s	secondary stream
sat	saturation
ss	conditions downstream of shock wave
sub	sub-cooling
t	total temperature/pressure
v	vapor
y	mixing section
1, 2, 3, 4	locations along the ejector

1. Introduction

The ejector refrigeration system has great market potential because it offers some remarkable advantages which include: (i) it can alleviate environment problems by using low grade thermal energy sources such as solar energy, geothermal energy and waste heat to drive the system instead of high grade electric energy, hence it can reduce CO_2 emissions resulting from the combustion of fossil fuels, (ii) it is simple and with no-moving parts, which makes it noise-free, reliable, long lifetime, low initial and running cost as well as require practically no maintenance and (iii) natural substances such as water can be utilized as working fluids, which have zero ozone depletion potential. The main flaws of the system are low performance efficiency and rigid requirements on the operation parameters which limits their widespread application. The most direct way to solve this problem is to investigate the ejector, which is the most critical component where highly irreversible transformations take place. In particular, due to its importance on the whole system, the ejector can be taken as the core of an optimization analysis aiming to define its operational conditions and the geometric configuration that make the COP of the system maximum [1]. Some review papers have been published to summarize the research efforts and achievements focused on ejector performance optimization. Chunnanond and Aphornratana [2] summarized the ejectors and their applications in refrigeration. They concluded that the understanding of the ejector theory had not been completely cleared. In order to enhance the efficiencies and reduce the cost of ejector cooling systems, efforts made by several researchers have been summarized in yet another review paper [3]. The review by Sun and Eames [4] outlined the developments in mathematical modeling and design of jet ejectors. However, the review considered only the thermodynamic model based on two basic approaches, the mixing of the primary fluid and the entrained fluid either at constant-pressure or at constant-area.

With the development of computer hardware and numerical methodology, mathematical models are being used for better understanding of the compression process, system design and performance evaluation considering the hydrodynamic performance, condensation and two-phase flow. The advantages of this method are that it takes less time and cost than experimental method for predicting the performance of an ejector. The second point is that mathematical models can produce large volumes of results at virtually no added expense and it is very convenient to perform parametric research and optimization analysis. The third reason is that by experimental means, some parameters are difficult to be obtained. The last but not the least reason is the fundamental physics of ejector used in various fields are similar, so that other installations may be investigated too by utilizing the model. Consequently, constructing valid mathematical models of the ejector has become the key subject of many studies. Lots of mathematical models have been constructed and employed to analyze, develop and design ejectors. This article examines the progress made in the area of mathematical modeling on the ejector, and summarizes comprehensively the numerous significant works that has been done on modeling the ejector.

Based on the conservation principles of energy, mass and momentum, the hydrodynamic and thermodynamic performance of ejector can be formulated with complex mathematical detail as governing equations and auxiliary relations. This is the main and universal method for constructing mathematical model. There are also some simplified models for ease of computation such as semi-empirical model [5]. Moreover, it is an effective way to get the empirical performance fitted correlation using large amounts of experimental results. But its application is restricted in the specific range of experimental working conditions. This paper focuses on the review of the mainstream mathematical models. Besides, some empirical/semi-empirical models are briefly introduced.

The first section of the paper details model establishment basis, which can be either thermodynamics or dynamics arranged according to the flowing phases. For each model reviewed, attempt has been made to gather the assumptions, governing equations, auxiliary relations and the solution techniques for ensuring the integrality of the model. The results and validation of some models are listed where comparison between them are needed.

2. Problem description

2.1. The fundamental principle

An ejector is also known as jet, injector or jet pump in different literatures. The main components of an ejector include a primary nozzle (also named as motive nozzle in some literatures), the suction chamber, the mixing chamber (including a convergent chamber if available and a constant-area throat tube which is named as secondary throat in some literatures) and the diffuser (Fig. 1).

The primary nozzle usually is a convergent–divergent nozzle. As the high pressure fluid, known as ‘‘a primary fluid’’ or ‘‘motive fluid’’, expands and accelerates through the primary nozzle, it flows out with supersonic speed to create a very low pressure region at the nozzle exit plane and subsequently in the mixing chamber. Hence, a pressure difference between the streams at the nozzle exit plane and the secondary fluid inlet is established and ‘‘a secondary fluid’’ or ‘‘entrained fluid’’ is drawn by the entrainment effect.

Based on Munday and Bagster’s theory [6], it is assumed that the primary fluid flows out without mixing with the secondary fluid immediately. It expands and forms a converging duct for the secondary fluid. At some cross-section along this duct, the speed of the secondary fluid increases to sonic value and chokes, were named as ‘‘hypothetical throat’’ (or ‘‘fictive throat’’ or ‘‘aero-dynamic throat’’ in some literatures). Then the mixing process begins after the secondary flow chokes (double-choking, critical-mode operation). It is assumed that the pressure of the two streams is uniform at the mixing section. Also, this mixing causes the velocity of the primary flow to be stepped down while the secondary flow is accelerated. By the end of the mixing chamber, the two streams are completely mixed and the static pressure is assumed to remain constant until it reaches the constant-area tube section. Due to a high pressure region downstream of the mixing chamber’s throat, the flow undergoes a succession of normal and/or oblique shock waves, also called a shock train, accompanied by a corresponding pressure rise. This shock causes a major compression effect and a sudden drop in the flow speed from supersonic to subsonic. A further compression of the flow is achieved as it is brought to stagnation through a subsonic diffuser.

It can be observed that due to the special geometrical structure of the ejector, the flow in the ejector is very complex, which involves supersonic flow, shock interactions, and turbulent mixing of two streams and two-phase flow in some cases. Hence the main endeavor of modeling the ejector is to reasonably explain the complex flow and mixing mechanism.

2.2. Flow and mixing mechanism in ejector

As mentioned in Section 2.1, the flow in the ejector can be divided into three sections:

(1) Nozzle section: A primary fluid is accelerated to supersonic speed by the convergent–divergent primary nozzle, which forms low pressure region at the nozzle exit plane and produces the entrainment effect to entrain the secondary fluid. Since the velocity is very high, the process can be considered as adiabatic and the isentropic relations are applicable.
(2) Mixing section: Two feasible mathematical methods, the constant-area mixing model and constant-pressure mixing model proposed by Keenan et al. [7] are used to describe the mixing mechanism. Also, a normal shock wave may occur if a supersonic fluid mixture enters the diffuser. In this case, a sudden reaction in the mixture velocity and a rise in the pressure take place. In addition, the fluid mixture easily undergoes phase change and a condensation shock may occur.
(3) Diffuser section: The mixture of primary and secondary flows passes through the diffuser, and converts kinetic energy into pressure energy. At the diffuser exit, the velocity is reduced to zero and the pressure is lifted high enough to cause discharge.

Therefore, the mathematical description of the flow inside the ejector is very complex. Besides the conservation equations of mass, energy and momentum, some gas dynamic equations, state equations, isentropic relations as well as some appropriate assumptions need to be used to assist in the description of the flow and mixing in the ejector.

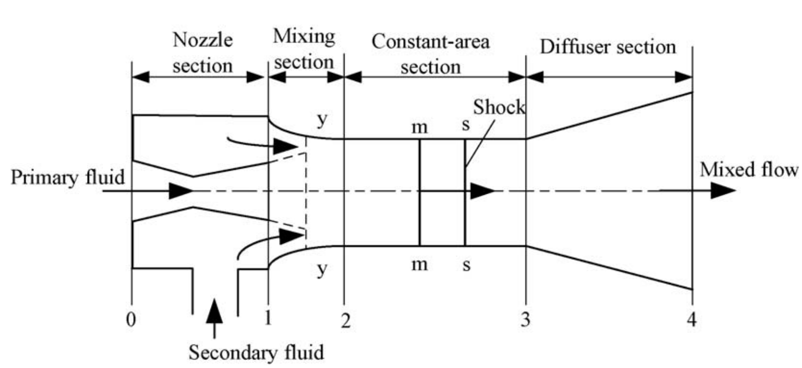


Fig. 1. Principle structure of ejector.

2.3. Mathematical model establishment

The main steps used to establish mathematical models include: (i) assumption proposal, (ii) deriving the governing equations based on the mass, energy and momentum balances, (iii) providing auxiliary relation to close the governing equations, and (iv) adopting proper mathematic approach to solve the model. For clarity, the system is considered to be one-dimensional (for thermodynamic models). Explanations of the main terms in the governing equations are presented below.

Some ideal assumptions are needed because the choking, shock and mixing of the two streams occurring in the ejector are too complicated to understand completely. On the other hand, some factors that do not influence the flow significantly can be neglected. Then the complexity of the governing equations can be reduced and the solution is relatively simple and time-saving. Some basic assumptions made before establishing mathematical models are as follows:

(1) The inner wall of the ejector is adiabatic.
(2) The flow inside the ejector is steady and isentropic.
(3) The primary fluid and secondary fluid are supplied to the ejector at zero velocity.
(4) The velocity at the ejector outlet is neglected.
(5) The two fluids begin to mix with a uniform pressure at the mixing section.

From assumption (1), the heat transfer between the ejector and the environment can be neglected and the isentropic expressions can be used based on assumption (2). Whereas from assumption (3), the inlet fluid is at a stagnant state, therefore, the inlet pressure and temperature of the fluid are also equal to the total pressure and temperature as well. From assumption (4), the fluid is brought down to stagnation when it discharges out of the ejector.

2.3.1. General governing equations

Under ideal condition, the general governing equations for the nozzle, mixing and diffuser sections are as follows:

$$\text{Conservation of mass}: \quad \sum \rho_i u_i A_i = \sum \rho_e u_e A_e \tag{1}$$

$$\text{Conservation of momentum}: \quad P_i A_i + \sum m_i u_i = P_e A_e + \sum m_e u_e \tag{2}$$

$$\text{Conservation of energy}: \quad \sum m_i (h_i + u_i^2/2) = \sum m_e (h_e + u_e^2/2) \tag{3}$$

2.3.2. Auxiliary conditions and mathematical methods

In order to close the equations, some auxiliary conditions have to be provided. They are boundary conditions, initial conditions for iteration, gas dynamic equations, entropy equation and the state equation. Also, the thermodynamic and transportation properties of the fluid should be given as well.

(1) Boundary conditions: Boundary conditions describe the behavior of the simulation at the edges of the simulation region. The boundary conditions commonly encountered in ejector models, are usually in pressures at inlet and exit of the ejector. Also the mass flow rates or the velocities of the primary and secondary fluids have been used as boundary conditions in some literatures.
(2) Initial conditions: The initial condition used in ejector models is the expansion ratio. The entrainment ratio and/or the cross-section area of the constant-area throat tube are also used for global models. In addition, the inlet conditions at the boundary mesh were used for local models.
(3) Turbulence modeling: As the flow in the ejector is from subsonic to sonic and then to supersonic, the turbulence has strong effect on the flowing process. Generally, for dynamic models, the Boussinesq hypothesis is used for turbulence (Eq. (4)). This means that they are based on an eddy viscosity assumption, which makes the Reynolds stress tensor resulting from equation averaging to be proportional to the mean deformation rate tensor.

$$-\rho\overline{u_i' u_j'} = \mu_t\left(\frac{\partial u_i}{\partial x_j} + \frac{\partial u_j}{\partial x_i}\right) - \frac{2}{3}\left(\rho k + \mu_t \frac{\delta u_i}{\delta x_i}\right)\delta_{ij} \tag{4}$$

For thermodynamic models, the turbulence cannot be modeled in detail. The dissipation term is interpreted by frictional and mixing losses which are taken into account by using corresponding coefficients introduced in the governing equations. Generally, these coefficients need to be determined experimentally.

(4) Auxiliary relations:

$$\text{Definition of Mach number}: \quad M = u/c \tag{5}$$

$$\text{Definition of sonic velocity}: \quad c = \sqrt{\left(\frac{\partial P}{\partial \rho}\right)_{is}}, \ \text{for ideal gas}, \quad c = \sqrt{\gamma R_g T} \tag{6}$$

Based on isentropic assumption, the following gas dynamic equations are frequently used in the thermodynamic models:

$$\frac{m}{A_i} = \frac{P_t\sqrt{\gamma_i}}{\sqrt{R_g T_t}} M_i \sqrt{\left(\frac{1}{1+\frac{\gamma_i-1}{2}M_i^2}\right)^{(\gamma_i+1)/(\gamma_i-1)}} \tag{7}$$

$$\frac{A_{i+1}}{A_i} = \frac{M_i}{M_{i+1}}\left[\frac{1+\frac{\gamma-1}{2}{M_{i+1}}^2}{1+\frac{\gamma-1}{2}{M_i}^2}\right]^{\frac{\gamma+1}{2(\gamma-1)}} \tag{8}$$

$$\frac{P_i}{P_{i+1}} = \left(\frac{1+\frac{r-1}{2}{M_{i+1}}^2}{1+\frac{r-1}{2}{M_i}^2}\right)^{\frac{r}{r-1}} \tag{9}$$

$$\frac{T_t}{T_{nt}} = 1 + \frac{\gamma-1}{2}M_{nt}^2 \tag{10}$$

$$\text{Entropy equation}: \quad \frac{P}{\rho^\gamma} = \text{constant} \tag{11}$$

$$\text{State equation}: \quad h = h(P, \rho) \tag{12}$$

$$\text{For constant pressure mixing}, \quad h = C_p T \tag{13}$$

(5) Mathematical solution: Due to the complexity and difficulty in modeling the flow in the ejector completely, most of the mathematical models are one-dimensional thermodynamic models which only calculate the steady-state explicit equations and obtains state and operation parameters along the ejector. Detailed information such as shock interactions, turbulent mixing of two streams cannot be obtained by these models. With the development of mathematical method and computer science, especially with the birth of commercial CFD software, numerical methods have been applied to solve the partial implicit differential governing equations which can give more information. At present, the most widely used solution

method for ejector model is finite difference method. The governing equations are solved using the commercial CFD software package FLUENT with the governing equations being discretized using a control volume technique.

3. Thermodynamic model

Among the different models, the model based on thermodynamic analysis is the simplest, which solve the equations in one dimension. In this model, the isentropic relations and some gas dynamic equations are used to assist in the description of the relationship between the temperature, pressure, enthalpy and Mach number and/or velocity. Hence, most of them are explicit steady-state models and work at design conditions.

Moreover, in order to simplify modeling, most of the models assume that the inlet fluid is superheated and no phase change occurring in the ejector. These models are developed based on single-phase flow. However, the experimental results indicate that the fluid in the ejector easily undergoes condensation shock. Also, for some practical application, the ejector works as a pump by using high pressure water to entrain gas or high pressure vapor to entrain water. In these cases, the flow in the ejector is two-phase flow. Therefore, in the next section, the models have been subdivided into single-phase flow models and two-phase flow models.

3.1. Single-phase flow model

3.1.1. Constant-pressure mixing model

Since the birth of the first steam jet refrigeration system, its advantages have made it to enjoy popularity. In 1942, the theoretical prediction of the ejector progressed further, when Keenan and Neumann [8] established a one-dimensional continuity, momentum and energy equations to predict the performance of the ejector. However, the difficulty in offering a reasonable analytical solution for the momentum conservation equation (Eq. (14)) during mixing, made the use some experimental coefficient necessary in model.

$$\sum F = \oint A dP = m_p(1+\omega)u_m - m_p u_{2p} - m_s u_{2s} \tag{14}$$

Therefore, in Keenan et al.'s following work [7], they introduced two feasible theoretical methods to solve the problem, the constant-pressure mixing model and the constant-area mixing model. The former considers that $dP = 0$ during mixing while the latter considers $dA = 0$.

Keenan et al.'s work lays a foundation for one-dimensional design theory of the ejector. They pointed out that a constant-pressure mixing ejector gives better performance than a constant-area mixing ejector. Therefore, most of the mathematical models that followed are based on the constant-pressure mixing ejector. However, Keenan et al.'s initial model could not give detailed information on the choking phenomena that is easy occurring in the supersonic ejector when the back pressure is low.

Munday and Bagster [6] further developed the constant-pressure mixing model by assuming that the primary fluid flows out without mixing with the secondary fluid immediately after discharging from the nozzle exit. They assumed that both fluids mix somewhere at the downstream of the nozzle exit (Fig. 1, section y–y) in the suction chamber and a "hypothetical throat" for entrained fluid is formed here.

However, neither Keenan's nor Munday's model has taken consideration of irreversibility due to friction. Eames et al. [9] modified Keenan's model to include irreversibility associated with the primary nozzle, mixing chamber and diffuser based on constant-pressure mixing theory but without considering the choking of the secondary flow. For simplification, besides assumptions (1–5) mentioned in Section 2.3, they further assumed:

(1) Friction losses were introduced by applying isentropic efficiencies to the primary nozzle, diffuser and mixing chamber.
(2) The two streams mixed at the primary nozzle exit plane.
(3) Mixing of the two streams is complete before a normal shock wave can occur at the end of the mixing chamber.
(4) The working fluid is ideal gas.
(5) The flow is one-dimensional.
(6) The constant-pressure mixing occurred at the inlet of the constant-area section (Fig. 2).

Based on these assumptions, the model was then written as:

Primary nozzle:

$$\text{Energy equation}: \quad \frac{u_{p1}^2}{2} = \eta_n(h_{p,t} - h_{p1}) \tag{15}$$

$$M_{p1} = \sqrt{\eta_n \frac{2}{\gamma-1}\left[\left(\frac{P_{p,t}}{P_1}\right)^{\frac{\gamma-1}{\gamma}} - 1\right]} \tag{16}$$

$$M_{s1} = \sqrt{\frac{2}{\gamma-1}\left[\left(\frac{P_{s,t}}{P_1}\right)^{\frac{\gamma-1}{\gamma}} - 1\right]} \tag{17}$$

where h_{p1} is the flow enthalpy at the nozzle exit for isentropic expansion.

Mixing section: Based on assumption (6), $P_1 = P_m$, $A_1 = A_m$, and assumption (5), the momentum equation (Eq. (2)) between section 1–1 and section m–m can be simplified into Eq. (18) with η_m as the efficiency for the whole mixing chamber.

$$\eta_m(m_p u_{p1} + m_s u_{s1}) = (m_p + m_s)u_m \tag{18}$$

Using Eq. (6), Eq. (18) then can be written in terms of the Mach number:

$$M_m^* = \frac{M_{p1}^* + \omega M_{s1}^* \sqrt{T_s/T_p}}{(\omega+1)(1+\omega T_s/T_p)} \tag{19}$$

where ω is the entrainment ratio: $\omega = m_s/m_p$, and $M^* = \sqrt{(\frac{\gamma+1}{2}M^2)/\left(1+\frac{\gamma-1}{2}M^2\right)}$, it is the actual mixture velocity divided by the sonic velocity of the mixture at critical conditions.

Shock wave: The relations between the Mach number and pressure lift upstream and downstream of the shock wave are

$$M_3 = \sqrt{\left(\frac{2}{\gamma-1} + M_m^2\right)/\left(\frac{2\gamma}{\gamma-1}M_m^2 - 1\right)} \tag{20}$$

$$P_3/P_m = \frac{1+\gamma M_3^2}{1+\gamma M_m^2} \tag{21}$$

Diffuser section: The pressure lift in the diffuser described in Mach number including η_d as efficiency is

$$P_4/P_3 = \left(\frac{(\gamma-1)\eta_d}{2}M_3^2 + 1\right)^{\frac{\gamma}{\gamma-1}} \tag{22}$$

Give the temperature, pressure and mass flow-rate of the primary and secondary fluids and assuming a value of $P_1/P_{s,t}$, calculating Eqs. (16), (17), (19–22) consequently, then you can

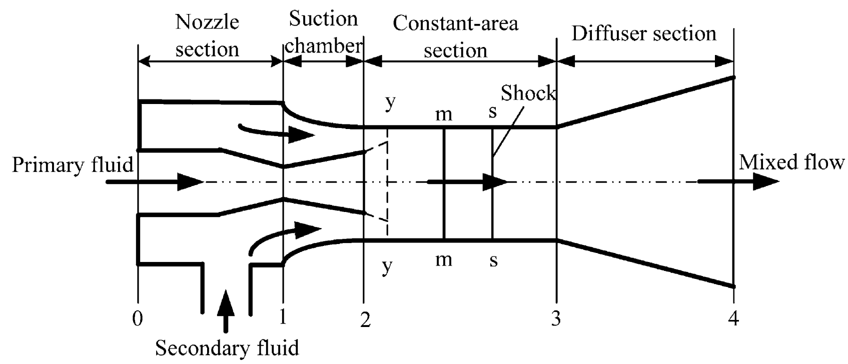


Fig. 2. Ejector model used by Eames et al.

obtain the exhaust pressure P_4, repeat the calculations with a new value of $P_1/P_{s,t}$ until the maximum P_4 is obtained. The primary nozzle, diffuser, and mixing chamber efficiencies of 0.85, 0.85 and 0.95, respectively were used for the analysis. The authors verified the theoretical results with experimental data and found that choking of the secondary flow in the mixing chamber of the ejector plays an important role in the system performance. Maximum COP can be obtained when the ejector is operated at its critical flow condition.

Based on the theory proposed by Munday and Bagster [6] and using the model developed by Eames et al. [9], Aly et al. [10] presented two models. One was developed by applying steady-state equations of energy, momentum and continuity at the nozzle, diffuser and mixing section to determine the pressure and velocity at each section from which the system performance can be obtained. Based on the assumptions (1–5) mentioned in Section 2.3 and taking into account of the losses due to wall friction in the nozzle, and those in the mixing and diffuser sections, the mathematical description of the model is as follows:

Primary nozzle:

$$\frac{u_{p1}^2}{2} = \eta_n(h_{p,t} - h_{p1}) \tag{15}$$

Mixing section: In the mixing section, both the momentum and energy balance equations were used. Comparing with Eq. (18), the momentum term of the secondary fluid at left side is omitted (Eq. (23)) based on assumption (3) in Section 2.3. The energy balance is shown in Eq. (24).

$$\eta_m m_p u_1 = (m_p + m_s) u_2 \tag{23}$$

$$(m_p + m_s)\left(h_2 + \frac{u_2^2}{2}\right) = m_s h_s + m_p\left(h_1 + \frac{u_1^2}{2}\right) \tag{24}$$

Shock wave: The Eq. (25) similar to Eq. (20) was derived to calculate the mixture velocity after the shock wave

$$u_3 = \sqrt{\left(\frac{2}{\gamma - 1} + M_2^2\right) \Big/ \left(\frac{2\gamma}{\gamma - 1} M_2^2 + 1\right)} \times c_3 \tag{25}$$

By applying the energy and continuity balance before and after shock wave, the enthalpy and density after the shock wave were

$$h_3 = h_2 + \frac{u_2^2}{2} - \frac{u_3^2}{2} \tag{26}$$

$$\rho_3 = \rho_2 \frac{u_2}{u_3} \tag{27}$$

Diffuser section: The energy equation taking account the isentropic efficiency for the diffuser section is

$$h_{4,is} = h_3 + \frac{u_3^2}{2\eta_d} \tag{28}$$

where $h_{4,is}$ is the flow enthalpy for the isentropic process.

Assuming a certain value for the entrainment ratio and considering the isentropic expansion process in the primary nozzle, the pressure P_1 and enthalpy h_1 at the nozzle exit can be obtained. Then Eqs. (15), (23–28) can be used to obtain the diffuser exit enthalpy h_4. The calculation is repeated with a new entrainment ratio until the required exit pressure is obtained.

The second model used the assumptions in the first model and in addition, the flow inside the ejector was considered as ideal gas with constant specific heat ratio both for the superheated region and the wet region separately. Following Eames et al.'s model of a steam–vapor ejector [9], they calculate the pressure ratio and Mach number of the flow in the ejector to study the characteristics of the system.

For validity, the results of the two models were compared with the empirical correlation of Power [11] and good agreement was found. Then both models were used to analysis the effect of the efficiencies such as nozzle and diffuser efficiencies, as well as the design parameters on the performance of the ejector. They found that the nozzle and diffuser efficiencies have a significant influence on the system performance.

In order to take account of the chocking of secondary fluid that neither Eames et al's nor Aly et al's models considered, Huang et al. [12] presented a critical-mode (double-chocking) model based on Munday and Bagster's theory [6] by assuming that the primary fluid mixed at some cross section (Fig. 2, section y–y) downstream of the nozzle exit. Hence, the model is more complex, besides all equations derived by Eames et al., the gas dynamic relations (Eqs. (6–10)) and state equation Eq. (13) were used in the calculation. In addition, the area relationship (Eq. (29)) and the energy conservation in mixing section (Eq. (30)) were used as well.

$$A_{py} + A_{sy} = A_3 \tag{29}$$

$$m_p\left(C_p T_{py} + \frac{u_{py}^2}{2}\right) + m_s\left(C_p T_{sy} + \frac{u_{sy}^2}{2}\right) = (m_p + m_s)\left(C_p T_m + \frac{u_m^2}{2}\right) \tag{30}$$

Eleven different ejectors were tested to determine the coefficients used in the model and to verify the theoretical analysis. Then the performance analysis was carried out to determine the entrainment ratio and the required cross sectional area of the constant-area throat tube. In this model, the initial

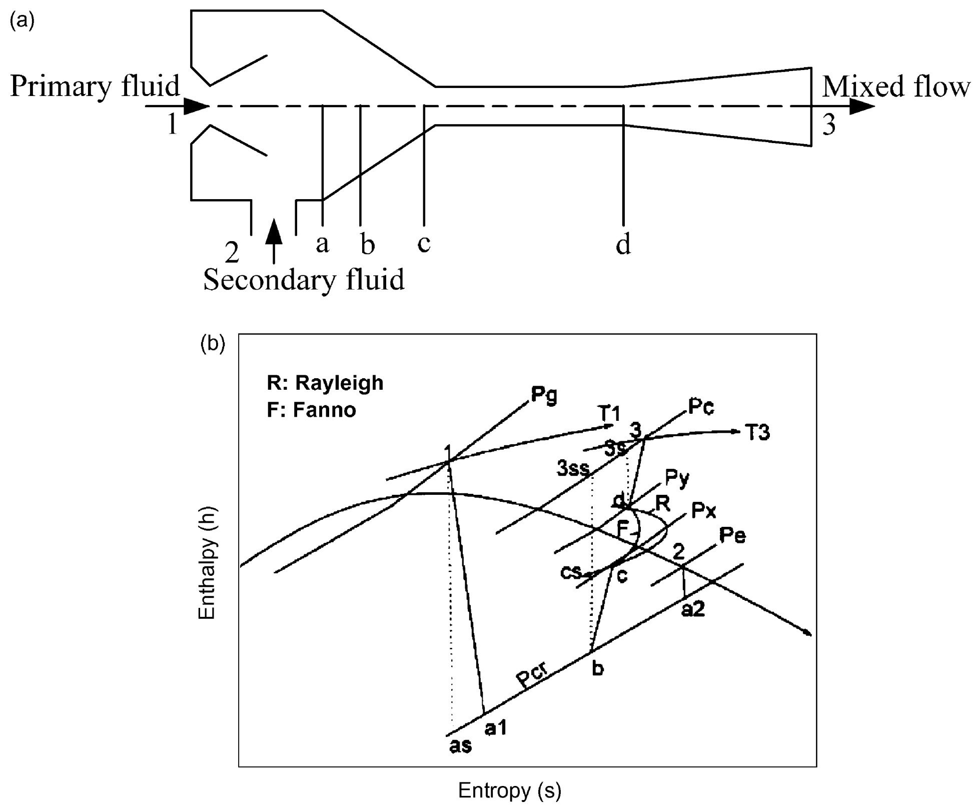


Fig. 3. Ejector and the Molier chart of an ammonia ejector.

conditions were the throat and exit area of the primary nozzle, the stagnant temperature and pressure of the primary and secondary fluid and the critical back pressure.

It should be pointed out that the previously mentioned models are based on ideal gas assumption which does not reflect the actual process occurring in the ejector. To solve this problem, Rogdakis and Alexis [13] improved the model proposed by Munday and Bagster [6] by using the thermodynamic and transportation properties of real gas. The model was based on the Molier chart of an ammonia ejector (Fig. 3(b)). The momentum conservation during mixing was employed in the model. Detailed governing equations are as follows:

Primary nozzle:

$$\text{The energy balance}: \quad u_{a1}^2/2 = h_1 - h_{a1} \tag{31}$$

$$\text{The state equation}: \quad s_1 = s(T_1, P_1) = s_{as} = x_{as}s_{gas} + (1 - x_{as})s_{fas} \tag{32}$$

and

$$h_{as} = x_{as}h_{gas} + (1 - x_{as})h_{fas} \tag{33}$$

$$\text{The isentropic efficiency is} \quad \eta_{1a1} = (h_1 - h_{a1})/(h_1 - h_{as}) \tag{34}$$

Similar equations were developed for the secondary fluid.

Mixing section:

$$\text{Momentum balance}: \quad u_{a1} + \omega u_{a2} = (1 + \omega)u_b \tag{35}$$

Similarly, by employing the energy balance and state equations Eqs. (31) and (32), the enthalpy h_c,h_d and the specific volume υ_c, υ_d can be obtained.

Diffuser section:

$$s_d = s(T_d, P_d) \tag{36}$$

$$s_{3s} = s_d = s(T_{3s}, P_d) \tag{37}$$

$$h_{3s} = h(T_{3s}, P_d) \tag{38}$$

$$n_{d3} = (h_d - h_{3s})/(h_d - h_3) \tag{39}$$

$$h_3 = h(T_3, P_3) \tag{40}$$

Given the pressure for the state (1–3) (Fig. 3(b)) and using iterative calculation, the maximum entrainment ratio ω can be found with constant superheated temperature T_1.

The ejector efficiency of compression is:

$$\eta = (m_g + m_e)(h_3 - h_2)/(m_g(h_1 - h_{as})) = (1 + \omega)(h_3 - h_2)/(h_1 - h_{as}) \tag{41}$$

The subscripts 1, 2, 3, b, c, d, a1, a2, as and 3s are the cycle locations as illustrated in Fig. 3.

The model can be used for one component or two components ejector. They used the model to analyse the performance of an ejector cooling system providing air conditioning and it was found that the shock phenomena on the entrained vapor play important role in ejector performance and the COP of the system. Also, from their work, they observed that the highest operating efficiency can be achieved if the generator pressure increases with decreasing condenser temperature, when the evaporator temperature is fixed. In addition, they showed that the maximum coefficient of performance is a linear function of generator temperature, a quadratic function of condenser temperature and a cubic function of evaporator temperature.

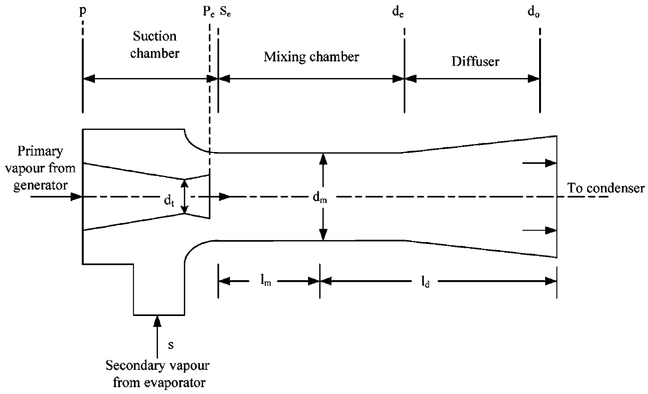


Fig. 4. Ejector model used by Selvaraju and Mani.

The friction loss is closely related with the velocity, and the velocity varies in a big range along the ejector. Therefore, using a constant coefficient to represent the friction loss as in above-mentioned models is a simplified treatment. Also, Aly et al. [10] found that the efficiencies have a significant influence on the system performance. Taking this into account, Selvaraju and Mani [14] developed a model based on Munday and Bagster's [6] theory for critical performance analysis of the ejector system (Fig. 4) by applying an expression to describe the friction loss in the constant-area section:

$$\frac{1}{\sqrt{f_m}} = 2.0\log(Re_m\sqrt{f_m}) - 0.8 \tag{42}$$

Then they derived the minimum area per mass flow rate and the velocity for both primary and secondary fluid at the primary nozzle outlet and the aerodynamic throat, respectively.

$$\frac{A_t}{m_p} = \frac{\upsilon_p}{\sqrt{2\eta_p(h_g - h_t)_{is}}} \tag{43}$$

$$u_{pe} = \sqrt{2\eta_p(h_g - h_{pe})}_{is} \tag{44}$$

The velocity of the mixed fluid is expressed as,

$$u_m = \frac{(m_p u_{pe} + m_s u_{me}) + (P_{se} - P_m)A_m}{m_m\left(1 + \frac{f_m}{2}\frac{l_m}{d_m}\right)} \tag{45}$$

The entrainment ratio and the characteristic area ratio for ejector are,

$$\omega = \frac{u_{pe} - u_{d1} - \frac{1}{2}u_{d1}f_m(l_m/D_m)}{u_{d1} - u_{se} + \frac{1}{2}u_{d1}f_m(l_m/D_m)} \tag{46}$$

$$\frac{A_m}{A_{nt}} = (1+\omega)\frac{\upsilon_m u_t}{\upsilon_p u_m} \tag{47}$$

The model was used to analyse the effect of the compression ratio and the driving pressure ratio on the critical entrainment ratio and to predict the performance of an ejector refrigeration system using various refrigerants. They found that the entrainment ratio is reversely proportional to the compression ratio, proportional with the driving pressure ratio, and the system with R134a gives better performance.

By using a model similar to that of Rogdakis and Alexis [13], Yu et al. [15] derived a thermodynamic model based on isentropic process to estimate the entrainment ratio of the ejector for both a refrigerator and a pump:

$$\omega = \sqrt{\eta_n\eta_m\eta_d((h_{p,t} - h_{p1})/(h_{md,s} - h_{mm}))} - 1 \tag{48}$$

where η_n,η_m and η_d are the efficiencies of the nozzle, mixing chamber and the diffuser. They can be obtained from the following expressions:

$$\eta_n = \frac{h_{p,t} - h_{p1}}{h_{p,t} - h_{p1,is}} \tag{49}$$

$$\eta_m = \frac{u_m^2}{u_{mp}^2} \tag{50}$$

$$\eta_d = \frac{h_{md,s} - h_{mm}}{h_{md} - h_{mm}} \tag{51}$$

This model was used to predict the ejector refrigeration system with mechanical sub cooling which uses an auxiliary liquid–gas ejector to enhance sub cooling for the refrigerant from condenser. It was found that the performance of this cycle improved more than the traditional ejector refrigeration system and an optimum mechanical sub-cooling degree exists for different refrigerant and operating conditions.

In order to obtain more detailed information on the ejector, Ouzzane and Aidoun [16] derived a local mathematical model and computer programs for ejector studies in refrigeration cycles, one program for optimal ejector design and the other for simulation with more in-built flexibility. The model is based on Munday and Bagster's theory [6] and isentropic flow in the nozzles and the diffuser. The control volume along the ejector axis is shown in Fig. 5. The conservation equations for the control volume are,

$$\text{Energy conservation}: \quad h_i + \frac{1}{2}u_i^2 = h_{i-1} + \frac{1}{2}u_{i-1}^2 \tag{52}$$

$$\text{Mass conservation}: \rho_i u_i A_i = \rho_{i-1}u_{i-1}A_{i-1} \tag{53}$$

$$\text{Isentropic condition}: \quad s_i = s_{i-1} \tag{54}$$

$$\text{Momentum conservation}: \quad \rho_i u_i^2 + P_i = \rho_{i-1}u_{i-1}^2 + P_{i-1} \tag{55}$$

The iteration variation for the solution procedure is Mach number, such that

$$M_i = M_{i-1} + \Delta M \tag{56}$$

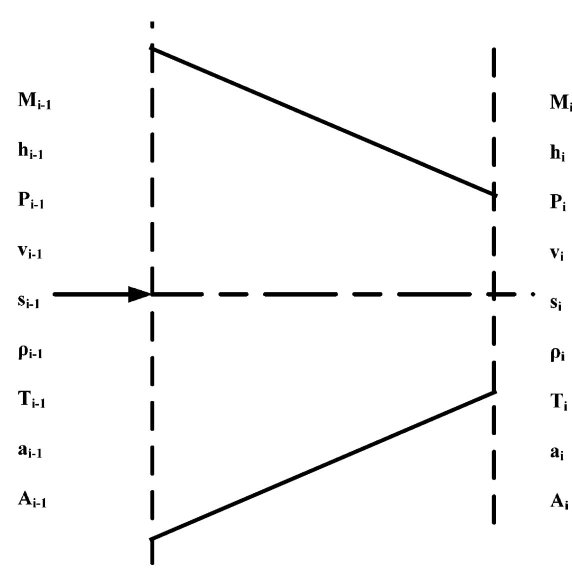


Fig. 5. Control volume used in Ouzzane and Aidoun's model.

The enthalpy value obtained from Eq. (52) is corrected for friction as:

$$h_i = h_{i-1} + \eta(h_{i,is} - h_{i-1}) \tag{57}$$

Together with the defining of Mach number and sonic velocity, and given the initial condition, the model can be calculated step by step.

The models were developed for qualitative and quantitative studies on the operation and performance for optimal and off design operation. The model can also be used to represent the global characteristics and detailed evolutions of all the relevant parameters. In addition, it can be used to study the influence of individual parameters on the general ejector operation. They used the model to analyze the effects of geometric configurations on ejector operation under different conditions showed that increasing ejector diameter improved entrainment ratios and capacities but exit pressures decreased accordingly. Component length affects not only the overall ejector size but also the capacity and the stream mixing process. The mixing chamber length was particularly important for the control of the shock wave intensity. Less irreversibility and limited superheat was produced in the ejector when the length was adjusted to bring supersonic mixed flow to near sonic conditions for maximum exit pressure. Hence, maximum isentropic compression was obtained in the supersonic convergent, greatly reducing the shock contribution, such that when combined with the pressure lift in the diffuser, the pressure at the ejector exit was globally higher.

3.1.2. Constant-area mixing model

Keenan and co-workers investigated the constant-area mixing ejector when they worked on the constant-pressure mixing model. They found that the constant-area mixing model offers better agreement with the experimental results than that of the constant-pressure mixing model. Also, the constant-area mixing model gives more information of the flow inside the ejector than that of the constant-pressure mixing model.

In the constant-area mixing model, except for the mixing method and the region, the assumptions made for the analysis of flow within the ejector are the same as those made in the case of one-dimensional constant-pressure ejector flow model.

The models proposed by Eames et al. [9] and Huang et al. [12] mentioned in Section 3.1.1 considered that the constant-pressure mixing occurred in the constant-area section. Therefore, both models are based on both constant-pressure mixing and constant-area mixing.

Grazzini and Mariani [17] derived a theoretical model based on the constant-area mixing theory. In their model, the following hypotheses were taken:

(1) Ideal gas behavior of the superheated steam.
(2) Same static pressure for primary and secondary flow at the nozzle exit plane section.
(3) Constant-area, adiabatic mixing process.
(4) Isentropic, one-dimensional, steady flow for both separated streams and for the mixed stream.
(5) Losses are introduced by means of the isentropic efficiency for the primary nozzle and the diffuser.

Using Eq. (16), the area ratio based on gas dynamic equation is:

$$\frac{A_1}{A_m} = \sqrt{\frac{1}{M_{p1}^2}\left(\frac{2}{\gamma+1}\left(1+\frac{\gamma-1}{2}M_{p1}^2\right)\right)^{(\gamma+1)/(\gamma-1)}} \tag{58}$$

With a recursive method to calculate the mass, momentum and energy balance equations using Mach number at the end section, the end thermodynamic variables at the ejector exit can be obtained using Eq. (7).

This model was developed for designing a jet pump device for a water refrigeration cycle. In order to improve the overall performance and the compactness of the system, they used the model to analyze a two-stage ejector which showed that the solution provides greater compression ratio while using the same entrainment ratio of the single stage jet pump. They also analyzed a jet pump with a third stage and found that the ideal gas model adopted could lose physical meaning.

In order to give a more accurate prediction of the performance, Yapici and Ersoy [18] derived a local model based on constant-area mixing ejector consisting of a primary nozzle, a mixing chamber in cylindrical structure and a diffuser (Fig. 6). The mathematical description of the model is as follows:

Primary nozzle: By using equations, such as (10), (13), (15), (49), and the mass flow rate at throat (Eq. (1)), they derived the following expressions to describe the primary nozzle pressure ratio (Eq. (60)) and the nozzle area ratio (Eq. (61))

$$m = \rho A u = PAM\sqrt{\frac{\gamma}{R_g T}} \tag{59}$$

$$\frac{P_{p1}}{P_{p0}} = \left[1 - \frac{1}{\eta_n} + \frac{1}{\eta_n\left(1+\frac{\gamma-1}{2}M_{p1}^2\right)}\right]^{\frac{\gamma}{\gamma-1}} \tag{60}$$

$$\frac{A_{p1}}{A_{p,nt}} = \frac{1}{M_{p1}}\left[\frac{1-\frac{\gamma-1}{2\eta_n+\eta_n(\gamma-1)}}{1--\frac{(\gamma-1)M_{p1}^2}{2\eta_n+\eta_n(\gamma-1)M_{p1}^2}}\right]^{\frac{\gamma}{\gamma-1}}\left[\frac{1+\frac{\gamma-1}{2}}{1+\frac{\gamma-1}{2}M_{p1}^2}\right]^{\frac{1}{2}} \tag{61}$$

Mixing section: For clarity, the control volume selected to analyze the flow in the mixing chamber is shown in Fig. 6. From

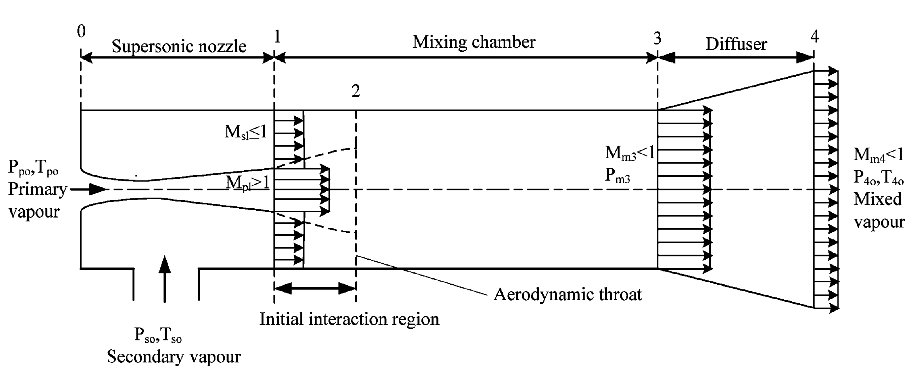


Fig. 6. Ejector model applied by Yapici et al.

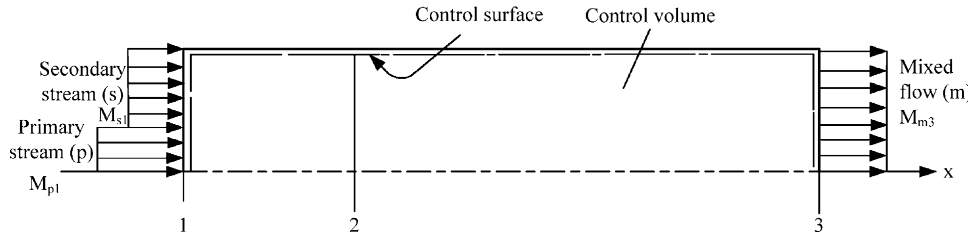


Fig. 7. Control volume selected to analyze the flow in the mixing chamber.

isentropic gas dynamic equation, the static pressure ratio P_{s1}/P_{p1} is,

$$\frac{P_{s1}}{P_{p1}} = \left(\frac{T_{s0}}{T_{p0}}\right)^{\frac{1}{2}} \left(\frac{A_{p1}}{A_{s1}}\right) \frac{f_2(\gamma, M_{p1})}{f_2(\gamma, M_{s1})} \omega \tag{62}$$

where $f_2(\gamma, M)$ is the mass flow function:

$$f_2(\gamma, M) = M\left[\gamma(1 + \frac{\gamma - 1}{2} M^2)\right]^{\frac{1}{2}} \tag{63}$$

Based on the continuity equation and energy balance for the selected control volume shown in Fig. 7, they derived:

$$\frac{P_{m3}}{P_{p1}} = \left(\frac{T_{m0}}{T_{p0}}\right)^{\frac{1}{2}} \left(\frac{A_{p1}}{A_{m3}}\right) \frac{f_2(\gamma, M_{p1})}{f_2(\gamma, M_{m3})} (\omega + 1) \tag{64}$$

$$\frac{T_{m0}}{T_{p0}} = (1 + \omega \frac{T_{s0}}{T_{p0}})/(1 + \omega) \tag{65}$$

$$\frac{P_{s0}}{P_{p0}} = \frac{P_{s1}}{P_{s0}} \frac{f_1(\gamma, M_{p1}, \eta_n)}{f_3(\gamma, M_{s1})} \tag{66}$$

where

$$f_3(\gamma, M) = \frac{P_{s1}}{P_{s0}} = \left[1 + \frac{\gamma - 1}{2} M_{s1}^2\right]^{\frac{-\gamma}{\gamma - 1}} \tag{67}$$

Considering that $\rho = P/(RT)$ and $u^2 = M^2 \gamma RT$, they derived the momentum equation in the x direction for the control volume (Eq. (68)) and the exit Mach number of the mixing chamber (Eq. (69)).

$$\frac{P_{s1}}{P_{p1}} \frac{A_{s1}}{A_{p1}} (1 + \gamma M_{s1}^2) + (1 + \gamma M_{p1}^2) = \frac{P_{m3}}{P_{p1}} \frac{A_{m3}}{A_{p1}} (1 + \gamma M_{m3}^2) \tag{68}$$

$$M_{m3} = \left[-(\alpha^2 - 2) \pm \left[(\alpha^2 - 2)^2 + 2\left(\frac{\gamma - 1}{\gamma}\right)\left(\alpha^2 - \frac{2\gamma}{\gamma - 1}\right)\right]^{\frac{1}{2}}\right]^{\frac{1}{2}} \left[(\gamma - 1)\left(\alpha^2 - \frac{2\gamma}{\gamma - 1}\right)\right]^{-\frac{1}{2}} \tag{69}$$

where

$$\alpha = \left\{ f_4(\gamma, M_{p1}) + \omega f_4(\gamma, M_{s1}) \left(\frac{T_{s0}}{T_{p0}}\right)^{\frac{1}{2}} \right\} \left\{ \left(\frac{T_{m0}}{T_{p0}}\right)^{\frac{1}{2}} (1 + \omega) \right\}^{-1} \tag{70}$$

$$f_4(\gamma, M) = \frac{1 + \gamma M^2}{M} \left[\gamma\left(1 + \frac{\gamma - 1}{2} M^2\right)\right]^{-\frac{1}{2}} \tag{71}$$

Fig. 8 shows the control volume for the initial interaction region of the mixing chamber. This control volume was used for analysis of the flow in the supersonic regime. In order to analyze the flow in this region, the following additional assumptions were made:

(1) Streams do not mix and are isentropic between sections 1–1 and 2–2;
(2) The secondary flow Mach number at section 2–2 is unity, $M_{s2} = 1$;
(3) The primary static pressure at the inlet is greater than that of the secondary, $P_{p1} > P_{s1}$

Considering that $A_{p2} = A_{m3} - A_{p1}$ and $A_{s1} = A_{m3} - A_{p1}$, together with Eq. (61), they derived

$$\frac{A_{p2}}{A_{p^*}} = \frac{\left[1 - \frac{1 - (A_{p1}/A_{m3})}{A_{s1}/A_{s2}}\right]}{A_{p1}/A_{m3}} \frac{1}{M_{p1}} \left(\frac{1 + \frac{\gamma - 1}{2}}{1 + \frac{\gamma - 1}{2} M_{p1}^2}\right)^{\frac{1}{2}} \left(1 - \frac{\gamma - 1}{\eta_n(\gamma + 1)}\right)^{\frac{\gamma}{\gamma - 1}} \left[1 - \frac{(\gamma - 1) M_{p1}^2}{2\eta_n + \eta_n(\gamma - 1) M_{p1}^2}\right]^{\frac{-\gamma}{\gamma - 1}} \tag{72}$$

In addition,

$$\frac{A_{p2}}{A_{p^*}} = \frac{1}{M_{p2}} \left(1 + \frac{\gamma - 1}{2} M_{p2}^2\right)^{\frac{\gamma + 1}{2(\gamma - 1)}} \left(1 + \frac{\gamma - 1}{2}\right)^{\frac{1}{2}} \left(1 - \frac{\gamma - 1}{\eta_n(\gamma + 1)}\right)^{\frac{\gamma}{\gamma - 1}} \left[1 - \frac{\eta_n - 1}{2\eta_n} (\gamma - 1) M_{p1}^2\right]^{\frac{-\gamma}{\gamma - 1}} \tag{73}$$

Thus, M_{p1} can be found by using the above two equations.

Considering that $M_{s2} = 1$ and $A_{s1} = A_{m3} - A_{p1}$, they derived the inlet static pressure ratio:

$$\frac{P_{s1}}{P_{p1}} = \frac{\frac{(P_{p2}/P_{p0})}{(P_{p1}/P_{p0})} \frac{(A_{p2}/A_{p^*})}{(A_{p1}/A_{p^*})} \left(1 + \gamma M_{p2}^2\right) - \left(1 + \gamma M_{p1}^2\right)}{\frac{1 - (A_{p1}/A_{m3})}{A_{p1}/A_{m3}} \left[\left(1 + \gamma M_{s1}^2\right) - \frac{P_{s2}/P_{s0}}{P_{s1}/P_{s0}} \frac{1 + \gamma}{A_{s1}/A_{s2^*}}\right]} \tag{74}$$

Diffuser section: By applying the Eq. (22) to calculate the diffuser pressure ratio, they derived the following expression for the pressure ratio through the ejector

$$\frac{P_{40}}{P_{s0}} = \frac{P_{40}}{P_{m3}} \frac{P_{m3}}{P_{p1}} \frac{P_{p1}}{P_{p0}} \frac{P_{p0}}{P_{s0}} \tag{75}$$

The authors derived the model for ejector optimization. Meanwhile, they carried out the parametric study by applying the model and derived the optimum design curves for constant-area ejector design. Further, they compared the analytical results with similar model developed by Sun and Eames [19] which was based on the constant-pressure mixing model, for the same operating temperatures of the ejector refrigeration system, and found the optimum coefficient of the performance and area ratio are greater.

3.2. Two-phase flow model

It should be pointed out that the above mentioned models are based on the assumption that the primary gas is superheated and the flow in the ejector is compressible single-phase flow and

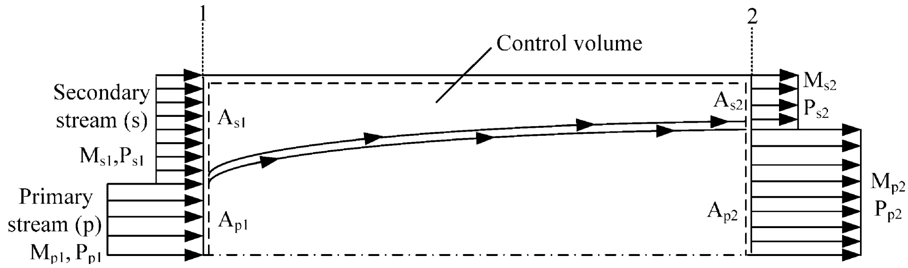


Fig. 8. A control volume selected for analysis of flow in the initial interaction region.

a normal shock wave may develop inside the diffuser. However, under many application conditions, the fluid mixture easily undergoes phase change and a condensation shock may develop. And because of the overall rise in pressure in the diffuser as well as the additional rise in pressure caused by the shock wave, the fluid mixture is easy to condensate. On the other hand, the secondary fluid will accelerate to sonic speed at the "hypothetical throat" which will reduce the pressure. Thus the sub cooled or saturated secondary fluid will flash into vapor and form either a two-phase mixture or pure vapor in the region occupied by the secondary fluid [20]. In addition, when the ejector works as a pump using high pressure liquid to entrain gas or higher pressure vapor to entrain liquid, under these cases, the flow is two-phase flow. Taking account of these cases, the models reviewed in this part are capable of properly simulating ejectors containing two-phase flow.

Sherif et al. [20] derived an isentropic homogeneous expansion/compression model to account for phase change due to expansion, compression and mixing while attempting to provide a more accurate description of the constant-pressure mixing process. In this model, the primary fluid is a two-phase mixture and the secondary fluid is either a sub-cooled or saturated liquid having the same chemical composition as the primary fluid. Therefore, comparing with single-phase flow model, the biggest difference in the model is the introduction of dryness of the fluid in the calculation of the specific volume, enthalpy and entropy. For clarity, the ejector model used by Sherif et al. is shown in Fig. 9.

Primary nozzle: Different from single-phase flow model, in the model, the primary nozzle is segmented into two parts, i.e. the converging section and the diverging section. For given inlet pressure, temperature and quality, the specific volume, enthalpy and entropy can be calculated by Eqs. (76)–(78).

$$\upsilon_{ni} = \upsilon_{ni,f} + x_{ni}(\upsilon_{ni,g} - \upsilon_{ni,f}) \tag{76}$$

$$h_{ni} = h_{ni,f} + x_{ni}(h_{ni,g} - h_{ni,f}) \tag{77}$$

$$s_{ni} = s_{ni,f} + x_{ni}(s_{ni,g} - s_{ni,f}) \tag{78}$$

Considering the continuity and energy equation in the converging section along with the definitions of the Mach number and the speed of sound, the isentropic flow requirement, and the equations of state, the enthalpy and density are,

$$\rho_{ni}A_{ni}u_{ni} = \rho_{nt}A_{nt}u_{nt} \tag{79}$$

$$h_{ni} + \frac{1}{2}u_{ni}^2 = h_{nt} + \frac{1}{2}u_{nt}^2 \tag{80}$$

$$s_{nt} = s_{ni} = s_{nt,f} + x_{nt}(s_{nt,g} - s_{nt,f}) \tag{81}$$

$$h_{nt} = h_{nt,f} + x_{nt}(h_{nt,g} - h_{nt,f}) \tag{82}$$

$$\frac{1}{\rho_{nt}} = \frac{1}{\rho_{nt,f}} + x_{nt}\left(\frac{1}{\rho_{nt,g}} - \frac{1}{\rho_{nt,f}}\right) \tag{83}$$

By assuming the pressure at the nozzle throat P_{nt} and using Eq. (81) to compute the quality at the throat x_{nt}. The quality can then be used to compute the specific enthalpy and density at the throat using Eqs. (82) and (83), respectively. And then the Eqs. (79) and (80) can be solved in the velocities u_m and u_{nt}. The speed of sound at the throat can be computed from Eq. (6) and be compared to the velocity term u_{nt}. If the two quantities are found different in value, another value of pressure is tried until convergence. Then

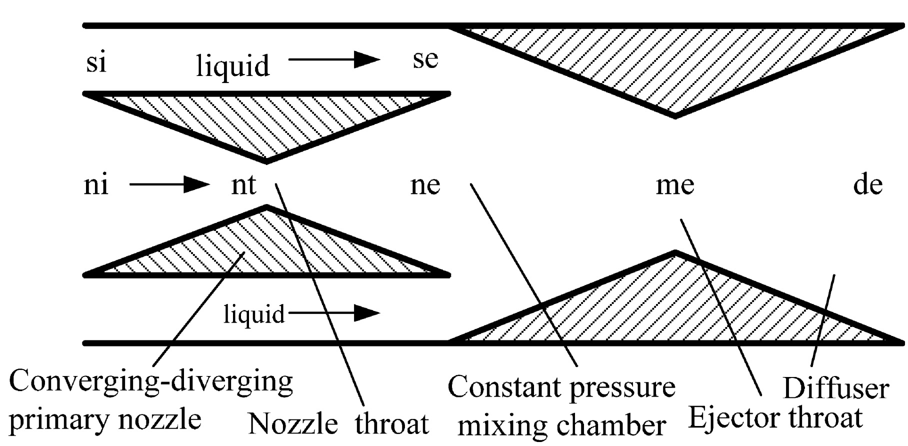


Fig. 9. Ejector model used by Sherif et al.

the mass flow rate of the primary fluid can be calculated by Eq. (59).

Using the same method by assuming the pressure at the nozzle exit, the state parameters at the nozzle exit can be solved.

Secondary flow: If the secondary flow is all liquid, Bernoulli's equation can be applied between the inlet and exit of the secondary flow tube,

$$P_{so} = P_{se} + \frac{1}{2}\rho_{so}u_{se}^2 \tag{84}$$

Assuming that the liquid density is nearly constant throughout the secondary fluid path, i.e. $\rho_{se} \approx \rho_{so}$, the secondary fluid flow rate can be calculated using Eq. (59).

For given entrainment ratio, Eqs. (84) and (59) can thus be solved to produce the pressure and velocity at the secondary flow path exit.

Mixing chamber: With the assumption of constant-pressure mixing, the continuity, momentum, and energy equations in the mixing chamber are

$$m_p(1+\omega) = \rho_{me}A_{me}u_{me} \tag{85}$$

$$(P_{ne} - P_{se})A_{ne} = m_p(1+\omega)u_{me} - m_p u_{ne} - m_p\omega u_{se} \tag{86}$$

$$(h_{ne} + \frac{1}{2}u_{ne}^2) + (h_{se} + \frac{1}{2}u_{se}^2)\omega = (h_{me} + \frac{1}{2}u_{me}^2)(1+\omega) \tag{87}$$

Similarly, the state parameters at the exit of the mixing chamber can be obtained by using the state equations similarly to Eqs. (81–83) as well as the equations defining the Mach number and the speed of sound.

Diffuser section: The conditions at the mixing chamber exit were assumed identical to those at the diffuser inlet and a shock wave is assumed to occur, then the mass, momentum and energy balance in the diffuser are,

$$\rho_{me}u_{me} = \rho_{ss}u_{ss} \tag{88}$$

$$P_{me} + \rho_{me}u_{me}^2 = P_{ss} + \rho_{ss}u_{ss}^2 \tag{89}$$

$$h_{me} + \frac{1}{2}u_{me}^2 = h_{ss} + \frac{1}{2}u_{ss}^2 \tag{90}$$

$$\rho = \rho(P, h) \tag{91}$$

Again, by assuming the pressure, the state parameters can be calculated using above equations.

For given entrainment ratio and inlet fluid states, the model can be used to determine the distribution of thermodynamic states as well as the area of the mixing chamber exit. By analyzing the performance of the ejector applying the model, the authors found that the variation of compression ratio with entrainment ratio follows a monotonically decreasing trend. The more energetic primary fluid appears to be more suitable for inducing high compression ratios than high entrainment ratios.

Cizungu et al. [21] derived a two-phase thermodynamic model to calculate the entrainment ratio shown in Eq. (92).

$$\omega = \frac{\sqrt{\frac{\Delta h_{exp}}{\Delta h_{com}}\eta_n\eta_d} - \left(1 + \frac{f_m}{2\xi_m}\frac{l_m}{d_m}\right)}{\left(1 + \frac{f_m}{2\xi_m}\frac{l_m}{d_m}\right) - \sqrt{\frac{\Delta h_{exs}}{\Delta h_{com}}\eta_s\eta_d}} \tag{92}$$

where f_m represents the friction factor, and ξ_m is the momentum loss factor, the enthalpy differences are given by $\Delta h_{exp} = h_{p0} - h_{p1,is}$ and $\Delta h_{exs} = h_{s,t} - h_{s1,is}$.The authors simplified the equations mentioned above for simple calculation:

$$\omega = \sqrt{\frac{\Delta h_{exp}}{\Delta h_{com}}\gamma} - 1 \tag{93}$$

where $\gamma = \eta_{exp}/\eta_{com}$ represents the quality grades of the jet compressor, it ranges between 0.689 and 0.81.

This model can be used both for single-phase flowing ejector and two-phase flowing ejector with single-component or two-component as the working fluid. For given boundary conditions the optimum geometry of the ejector can be calculated. For given geometry of the ejector, the optimum thermal conditions can be determined. They used the model to analysis the interaction between the entrainment ratio and all relevant dimensional parameters and compared the results with experimental data. Good agreement was found. They also found that the dimensions of ejector configuration have a dominant influence in deciding the operating range.

Another kind of widely used two-phase flowing ejector is that employs liquid as primary fluid and gas as secondary fluid or vice versa. This kind of ejector found widely application in industry, such as steam-driven jet pump used in modern thermal power plant to remove non-condensable gases from the condenser, ejectors used to entrain and pump fumes and dust-laden gases which otherwise are difficult to handle and so on. Therefore, Beithou and Aybar [22] employed a one-dimensional control volume method to develop a local mathematical model for the performance prediction of the steam-driven jet pump. In the model, the conservation of mass and momentum equation as well as the entropy equation were applied. As the fluid is uncompressible, therefore, the Bernoulli equation can be used to calculate the entrained water velocity at the nozzle. Regarding to the mixing section, the steady-state energy equation was used to calculate the velocity of the mixture with the assumption of adiabatic mixing process as well of no potential energy change. Take the head loss into account, the Bernoulli equation was used in the diffuser to find out the pressure and velocity profiles along it. The mathematical model is shown as follows.

Steam nozzle:

$$\text{Conservation of mass}: \quad \sum \rho_i u_i A_i = \sum \rho_e u_e A_e \tag{1}$$

$$\text{Conservation of momentum}: \quad \rho\frac{\partial u}{\partial t} + \rho u\frac{\partial u}{\partial x} + \frac{\partial P}{\partial x} = 0 \tag{94}$$

The governing equations of steady-state subsonic or supersonic isentropic flow:

$$\frac{d}{dx}(\rho u A) = 0 \tag{95}$$

$$u\frac{du}{dx} + \frac{1}{\rho}\frac{dP}{dx} = 0 \tag{96}$$

Also the entropy equation Eq. (11) is used.

Water nozzle:

By using Bernoulli equation between the water tank and the exit of the water nozzle and the continuity equation, the water velocity and water flow rate can be calculated by Eqs. (97) and (59):

$$u_{wc} = \sqrt{2\left(\frac{P_T}{\rho_T} - \frac{P_c}{\rho_{wc}}\right)} \tag{97}$$

where, the subscript "T" defines the water properties in the supply water tank, and the subscript "wc" shows the water properties at the inlet of water nozzle.

Mixing section: The steady-state energy equation with assumption of no potential energy change is similarly to Eq. (30).

Diffuser section: Applying Bernoulli and considering the head loss, they derived:

$$\frac{u_d^2}{2}+\frac{P_d}{\rho_d}=\frac{u_e^2}{2}+\frac{P_e}{\rho_e}+h_L \tag{98}$$

where h_L is the head loss which is given by,

$$h_L=\frac{u_d^2}{2}\left[1-(\frac{A_d}{A_e})2-\eta_p\right] \tag{99}$$

where η_p is the pressure recovery coefficient.

In the steam nozzle, the iterative finite difference procedure with under-relaxation is used to approximate the derivatives in the steam nozzle governing equations that are expressed in terms of the mesh points.

The initial condition is the state parameters and geometrical parameter of the inlet section of the steam subsonic nozzle. The nozzle shape is such that the area variation with distance along the nozzle is given by a quadratic function. In the subsonic nozzle, the effect of the density changes is negligible. Assuming $\rho_i = \rho_1$ gives the initialization of density at every grid point, and then calculates the velocity and the pressure at each grid point for the first iteration by,

$$u_i=\frac{\rho_1 u_1 A_1}{\rho_i A_i} \tag{100}$$

$$P_i=P_{i-1}-\rho_i u_i(u_i-u_{i-1}) \tag{101}$$

$$\rho_i^{n+1}=\rho_i^n+r\left[\rho_1(\frac{P_i}{P_1})^{1/\gamma}-\rho_i^n\right] \tag{102}$$

where the index 1 shows the initial condition, n shows the density at the previous iteration, and the under-relaxation factor r is to be chosen less than 1. Then the pressure, velocity and density can be updated by following equations:

$$P_i=P_1\left(\frac{\rho_i}{\rho_1}\right)^{\gamma} \tag{103}$$

$$u_i=u_{i-1}-\left[\frac{(P_i-P_{i-1})}{\rho_i u_i}\right] \tag{104}$$

$$\rho_i^{n+1}=\rho_i^n+r\left[\frac{\rho_1 u_1 A_1}{u_i A_i}-\rho_i^n\right] \tag{105}$$

The goal of the model is to evaluate the pressure, density and velocity distribution along the ejector. The heat transfer rate from steam to water was obtained using the direct-contact heat transfer coefficient as a function of the length of a conical steam jet plume. The condensation profile, non-condensed steam percentage in volume versus non-dimensional length of mixing section was obtained from the heat transfer rate profile. They compared the calculated pressure profile of the model with Cattadori et al.'s [23] experimental pressure profile which found that the experimental and calculated pressure distributions are in good agreement in the mixing nozzle and diffuser, and there are some difference in steam nozzle.

The above mentioned local model models the flow in the injector at each point, and taking into account major phenomena such as condensation of droplets, heat and momentum transfers, viscous dissipation on the wall non-adiabatic and non-equilibrium flow. Such a model is more realistic, but needs a perfect knowledge of the previously mentioned phenomena as well as their mutual interactions that makes the model very complex. Take these in consideration, Deberne et al. [24] derived a global volume model (Fig. 10) for steam ejector performance with the consideration of void fraction, area contraction ratio and condensation rate in the conservation of mass, momentum and energy equations based on steady and one-dimensional assumption.

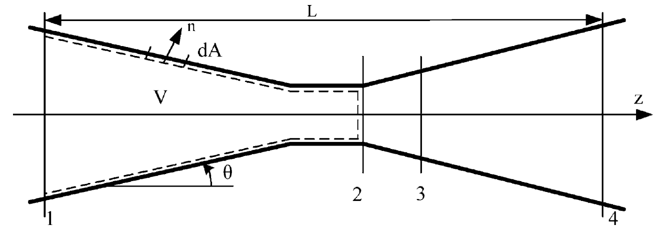


Fig. 10. Control volume for the modeling of the mixing chamber.

By defining the following parameters:

$$\text{Void fraction}: \quad \varepsilon_1=\frac{1}{\left(\omega\frac{\rho_{1s}u_{1s}}{\rho_{1l}u_{1l}}+1\right)} \tag{106}$$

$$\text{Area contraction ratio}: \quad \Omega=\frac{A_2}{A_{1s}+A_{1l}} \tag{107}$$

$$\text{Condensation rate}: \quad R=\left(\frac{x_1 L_v}{C_{p1}\Delta T\omega}\right)_{P_1} \tag{108}$$

The conservation equations applied to the global volume lead to:

$$\text{Mass}: \quad \rho_2 u_2=(1+\omega)\frac{1}{\Omega}\varepsilon_1\rho_{1s}u_{1s} \tag{109}$$

$$\text{Momentum}: \quad (1+\omega)u_2+\frac{\Omega}{\varepsilon_{1s}\rho_{1s}u_{1s}}\left(P_2+\left(1-\frac{1}{\Omega}\right)P^*\right) = (u_{1s}+\omega u_{1s})+\frac{P_{1s}}{\varepsilon_1\rho_{1s}u_{1s}} \tag{110}$$

$$\text{Energy}: \quad (1+\omega)\left[h_2+\frac{u_2^2}{2}\right]=\omega\left[h_{1l}+\frac{u_{1l}^2}{2}\right]+\left[h_{1s}+\frac{u_{1s}^2}{2}\right] \tag{111}$$

$$\text{State equation}: \quad h_2=h(P_2,\rho_2) \tag{12}$$

where the equivalent pressure P^* are obtained by the empirical correction numerically introduced from the experiment results at the CETHIL:

$$P^*=1.01R^{2.572}\times P_{1s} \tag{112}$$

wherein, the subscript of 1s refers to mixing section inlet. The subscripts 1l and 2, respectively, denotes the water mixing section inlet (water nozzle outlet), the mixing section outlet planes. $\Delta T = T_{sat} - T_{1l}$ (T_{sat} is saturation temperature at pressure P) is the inlet liquid sub cooling, L_v is the latent heat of water, C_{pl} is the heat capacity of liquid and x_1 is the vapor quality at the mixing inlet section.

Shock wave:

They discussed the shock wave under two conditions: (i) too high void fraction, the fluid will not be condensed enough to reach a complete condensation across the shock wave and (ii) the void fraction is too low, the fluid velocity will be too low (lower than the sound speed) and no shock wave can occur.

The first sound speed corresponds to the case where response of droplets is negligible (droplets are frozen with no mass and momentum transfers), and is similar to the sound speed in pure gases:

$$c_f=\sqrt{\gamma R_g T_s} \tag{113}$$

The other sound speed, presented in Young and Guha [25] is called the full equilibrium sound speed, where all processes are in equilibrium during shock wave:

$$c_e = \sqrt{\frac{x\gamma R_g T_s}{\gamma\left[1 - \frac{R_g T_s}{L_v}\left(2 - \frac{cT_s}{L_v}\right)\right]}} \tag{114}$$

where $c = c_{ps} + ((1-\varepsilon)/\varepsilon)c_{pl}$, in the model, the normal shock wave is consider in full normal shock wave, fully dispersed with discontinuity in flow properties and partly dispersed shock wave. For shock wave, and neglect the effect of the wall on the wave, surface area of sections 2–2 and 3–3 are taken to be equal, and then the conservation equations are as follows:

$$\text{Mass}: \quad \rho_3 u_3 = \rho_2 u_2 \quad \text{with} \quad \rho_2 = \varepsilon\rho_{2s} + (1-\varepsilon)\rho_{2l} \tag{115}$$

$$\text{Momentum}: \quad \rho_3 u_3^2 + P_3 = \rho_2 u_2^2 + P_2 \tag{116}$$

$$\text{Energy}: \quad \rho_3 u_3\left(h_3 + \frac{1}{2}u_3^2\right) = \rho_2\frac{u_2^2}{2} + u_2[\varepsilon_2\rho_{2s}h_{2s} + (1-\varepsilon_2)\rho_{2l}h_{2l}] \tag{117}$$

$$\text{State equation}: \quad h_3 = h(P_3, \rho_3) \tag{12}$$

Diffuser: By introducing a pressure loss term in the Bernoulli equation, then the Bernoulli equation is,

$$P_4 + \frac{1}{2}\rho_3 u_4^2 = P_3 + \frac{1}{2}\rho_3 u_3^2 - \eta_d\rho_3 u_3^2 \tag{118}$$

Once the inlet conditions are known, as well as the steam injector geometry, the condensation rate R is calculated. The term P^* is calculated with the equivalent pressure ratio τ^* and then all the other constants. If no solution for the system of Eqs. (116) + (12) + (117) + (118) can be found, the calculation aborts if the flow velocity u_2 is lower than sound speed upstream of the shock wave to ensure the assumption (two-phase supersonic upstream flow, shock wave and liquid downstream flow). Physical quantities of the flow are then calculated upstream and downstream of the shock wave and the minimum void fraction condition is a posteriori verified (to be sure that a normal shock wave exists). The outlet quantities are, in this case, calculated.

The authors also set up a test rig to verify the model and 15% performance prediction accuracy had been found. Then a series of parametric investigation were carried out by applying the model to predict the influence of different geometrical parameters of the ejector (mixing section throat diameter, position of the liquid pipe, etc.) and the influence of physical parameters (temperature, liquid and steam pressure, etc.) on the ejector performance.

The thermodynamic models summarized in this part are reviewed in Table 1.

4. Dynamic model

Despite the usefulness and the remarkable progress the thermodynamic models provided for the general understanding of ejectors, this kind of models were unable to correctly reproduce the flow physics locally along the ejector. It is the understanding of local interactions between shock waves and boundary layers, their influence on mixing and recompression rate, that will allow a more reliable and accurate design, in terms of geometry, refrigerant type and operation conditions. A way of achieving this objective at a reasonable cost is through computational fluid dynamics (CFD) modeling approach which provides a better understanding of the hydrodynamics of the ejector. Such models are called dynamic model (listed in Table 2). Although dynamic model needs more time compared with thermodynamic model, it is more related to the true physics of the problem. Therefore, dynamic model is likely to give better agreement with experiment results. With the development of computer science and mathematical method, more and more researchers have focused on this method with attempt to obtain more accurate information in the ejector.

4.1. Single-phase flow model

The single-phase flow model includes gas-gas ejector and liquid-liquid ejector flow model. The former considers the flow as compressible while the latter as incompressible.

Because of poor mesh resolution, the early CFD models [26–28] are failed to track the shock wave and poor agreement with the experimental results. Rusly et al. [29] simulated the flow through an R141b ejector by using the real gas model in the commercial code, FLUENT. The effects of ejector geometries were investigated

Table 1
Features of thermodynamic model reviewed in present work.

Ref.	Media	Gas property	Multiphase flow model	Mixing section	Mixing mechanism				B.C.[d]	I.C.[e]	Other relations
		Ideal gas	Real gas		NXP[a]	Section y–y	CPM[b]	CAM[c]			
[9]	Steam	√		Compressible single-phase	√		√	√	T_p, P_p, m_p, T_s, P_s, m_s	$P_1/P_{s,t}$	Eqs. (15–21)
[10]	Steam	√		Compressible single-phase			√		T_p, P_p, T_s, P_s	ω	Eqs. (15), (23–28)
[12]	R141b	√		Compressible single-phase		√	√	√	$T_p, P_p, T_s, P_s, P_e^*, A_t$	A_{nt}, A_1	Eqs. (6–10), (13), (29), (30)
[13]	R717		√	Compressible single-phase		√	√		T_1, T_2, T_3		Eqs. (31–41)
[14]	R134a[*]		√	Compressible single-phase		√	√		T_p, P_p, T_s, P_s, P_e		Eqs. (42–47)
[15]	R142b		√	Compressible single-phase		√	√		Inlet conditions		Eqs. (48–51)
[16]	R142b		√	Compressible single-phase		√	√		Inlet conditions	P	Eqs. (5), (6), (52–57)
[17]	Steam	√		Compressible single-phase	√		√	√	T_p, P_p, T_s, P_s		Eqs. (1)–(3), (7), (16), (58)
[18]	R123		√	Compressible single-phase		√	√	√	T_p, T_s, T_e		Eqs. (10), (13), (15), (49), (59–75)
[20]	R134a		√	Homogeneous model			√		T_p, P_p, T_s, P_s	P_{nt}, P_{y1}	Eqs. (6), (59), (76–91)
[21]	NH_3		√	Two-phase					T_p, T_s, T_e		Eqs. (92), (93)
[22]	Steam–water			Condensation					Inlet conditions		Eqs. (1), (11), (30), (94–105)
[24]	Steam			Condensation			√		Inlet conditions		Eqs. (12), (109–118)

[a] NXP: nozzle exit plane.
[b] CPM: constant-pressure mixing.
[c] CAM: constant-area mixing.
[d] B.C.: boundary conditions.
[e] I.C.: initial conditions.
[*] Other media used are R152a, R290, R600a, R717.

Table 2
Features of dynamic model reviewed in present work.

Ref.	Media	Gas property		Multiphase flow model	Turbulence model	Mixing mechanism			Other relations
		Ideal gas	Real gas			CPM	CAM	B.C.	
[29]	R141b		√	Compressible single-phase	Realizable k-ε	√		T_p, T_s, T_e	Eqs. (4), (119–122)
[31]	Air	√		Compressible single-phase	RNG k-ε, SST, k-ω	√		T_p, P_p, T_s, P_s, P_e	Eqs. (4), (119–126)
[34]	R142b		√	Compressible single-phase	k-ε, SST, k-ω	√		T_p, P_p, T_s, P_s, P_e	Eqs. (4), (119–126)
[35]	R141b		√	Compressible single-phase	RNG k-ε	√		P_p, P_s, P_e	Eqs. (4), (119–124)
[36]	Steam	√		Compressible single-phase	Realizable k-ε	√	√	P_p, P_s, P_e	Eqs. (4), (119–124)
[37]	Water–air		Air	ASM	Standard k-ε			u_p, P_s, P_e	Eqs. (124), (127–130)
[38]	Water–air		Air	Mixture				u_p, P_s, P_e	Eqs. (127–130)
[39]	Water–air		Air	ASM Eulerian	Standard k-ε			u_p, P_s, P_e	Eqs. (127–133)
[41]	Air–water		Air	mixture	Standard k-ε			m_p, m_s, P_e	Eqs. (127–130)
[42]	Water–vapor			Separated two-phase				P_p, T_p, P_s, x	Eqs. (134–149)

numerically. The CFD's results were validated with experimental data provided by others [12] and good agreements were found.

As it is often the case in transonic compressible flows involving shock reflections and shock-mixing layer interaction, the choice of the turbulence model and grid refinements are critical points [30]. Therefore, Bartosiewicz et al. [31] used the CFD model aiming at validating the choice of a turbulence model for the computation of supersonic ejectors in refrigeration applications. In order to reduce the complexity of the model and to be able to use the available experimental data, they chose air as the working fluid. Six turbulence models, named k-ε, realizable k-ε, renormalization-group (RNG) k-ε, RSM and shear-stress transport (SST) k-ω have been tested and compared with measurements of Desevaux and Aeschbacher [32] and Desevaux et al. [33]. The compressible steady-state axisymmetric form of the fluid flow governing equations are shown as Eqs. (119–122) together with ideal gas law Eq. (123).

$$\text{Conservation of mass}: \quad A\frac{\partial \rho}{\partial t} + \frac{\partial}{\partial x_i}(\rho u_i A) = 0 \tag{119}$$

$$\text{Conservation of momentum}: \quad \frac{\partial}{\partial t}(\rho u_i) + \frac{\partial}{\partial x_j}(\rho u_i u_j) = -\frac{\partial P}{\partial x_i} + \frac{\partial \tau_{ij}}{\partial x_j} \tag{120}$$

$$\text{Conservation of energy}: \quad \frac{\partial}{\partial t}(\rho E) + \frac{\partial}{\partial x_i}(u_i(\rho E + P)) = \vec{\nabla}\left(\alpha_{eff}\frac{\partial T}{\partial x_i}\right) + \vec{\nabla}(u_j(\tau_{ij})) \tag{121}$$

with

$$\tau_{ij} = \mu_{eff}\left(\frac{\partial u_i}{\partial x_j} + \frac{\partial u_j}{\partial x_i}\right) - \frac{2}{3}\mu_{eff}\frac{\partial u_k}{\partial x_k}\delta_{ij} \tag{122}$$

$$\rho = \frac{P}{RT} \tag{123}$$

As the k-ε, RNG k-ε and k-ω models are based on the Boussinesq hypothesis which makes these approaches need relatively low computational cost associated with the determination of the turbulent viscosity. However, the main drawback of the approach is the assumption that the turbulence is isotropic. While the Reynolds stress model (RSM) does not rely on the Boussinesq assumption, but the associated CPU cost is relatively high. Comparing the vast simulations by applying these approaches, Bartosiewicz and his coworkers found that the RNG k-ε and SST k-ω models were very promising for ejector analysis. Therefore, they compared these two approaches in detail.

The RNG-k-ε model (RNG)

$$\frac{\partial}{\partial x_i}(\rho \varepsilon u_i) = \frac{\partial}{\partial x_j}\left[\alpha_\varepsilon \mu_{eff}\frac{\partial \varepsilon}{\partial x_j}\right] + C_{1\varepsilon}\frac{\varepsilon}{k}G_k - C_{2\varepsilon}\rho\frac{\varepsilon^2}{k} - R_\varepsilon \tag{124}$$

With $R_\varepsilon = \frac{C_\mu \rho \eta^3(1-\eta/\eta_0)}{1+\beta\eta^3}\frac{\varepsilon^2}{k}$, $\eta = Sk/\varepsilon$, $\eta_0 = 4.38$, $\beta = 0.012$, $C_{1\varepsilon} = 1.42$, $C_{2\varepsilon} = 1.68$, $C_\mu = 0.0845$, and $\mu_t = \rho C_\mu(k^2/\varepsilon)$.

The standard and SST k-ω models

$$\frac{\partial}{\partial t}(\rho\omega) + \frac{\partial}{\partial x_i}(\rho\omega u_i) = \frac{\partial}{\partial x_j}\left[\left(\mu + \frac{\mu_t}{\sigma_\omega}\right)\frac{\partial \omega}{\partial x_j}\right] + G_\omega - Y_\omega \tag{125}$$

With $\mu_t = \varepsilon^* \frac{\rho k}{\omega}$ and

$$\frac{\partial}{\partial t}(\rho\omega) + \frac{\partial}{\partial x_i}(\rho\omega u_i) = \frac{\partial}{\partial x_j}\left[\left(\mu + \frac{\mu_t}{\sigma_\omega}\right)\frac{\partial \omega}{\partial x_j}\right] + G_\omega - Y_\omega + (1 - F_1)D_\omega \tag{126}$$

The investigation has shown that the RNG k-ε and SST k-ω models were the best suited to predict the shock phase, strength, and the mean line of pressure recovery with the SST k-ω model shown better performances in term of stream mixing.

Then they used the validated model to reproduce the different operation modes of a supersonic ejector, ranging from on-design point to off-design to capture the shock-boundary layer interactions, such as boundary layer separation, flow separation and recirculation at the motive nozzle exit and the diffuser. The results turned out that CFD is an efficient diagnosis tool of ejector analysis (mixing, flow separation), for design, and performance optimization (optimum entrainment and recompression ratios).

In Bartosiewicz et al.'s [34] work, they improved the previously mentioned model by using real gas thermodynamic and transportation properties derived from NIST-REFPROP database to perform simulation studies on ejector operation with R142b. They observed over-expanded and a strong oblique shock at the primary nozzle exit which induces a mixing layer separation associated with a corresponding energy loss. Consequently, this separation creates an adverse pressure gradient at the secondary inlet, giving rise to favorable conditions for an outflow. The one-dimensional model cannot take into account such irreversible losses induced by oblique shock wave reflection and flow separation. This local CFD modeling takes into account shock-boundary layer interactions in a real refrigerant. The numerical results contribute to understanding the local structure of the flow and demonstrate the critical role of the secondary nozzle for the mixing rate performance.

Zhu et al. [35] employed the CFD technique with RNG k-ε model to investigate the effects of two important ejector geometry parameters: the primary Nozzle Exit Position (NXP) and the mixing section converging angle θ, on its performance. The flow inside the ejector is governed by the compressible steady-state turbulent form of the flow governing equations. They found that the optimum NXP is not only proportional to the mixing section throat diameter, but also increases as the primary flow pressure rises. On the other hand, the ejector performance is very sensitive to θ especially near the optimum working point. The entrainment ratio varies as much as 26.6% by changing θ. In order to better maximize the ejector performance, a relatively biggerθ is required when the primary flow pressure rises. These findings are good for guiding the adjustment of NXP and θ in order to obtain the best ejector system performance when the operating conditions are different from the on-design conditions.

The previously mentioned dynamic models are based on constant-pressure mixing ejector. Pianthong [36] employed the CFD with realizable k-ε turbulence model to predict the flow phenomena and performance of both constant-pressure mixing and constant-area mixing steam ejectors with application in refrigeration system. The results indicate that CFD can predict ejector performance very well and reveal the effect of operating conditions on the effective area that is directly related its performance. Besides, they found that the flow pattern does not depend much on the suction zone because the results of axisymmetric and 3D simulation are similar.

4.2. Two-phase flow model

There are two approaches for the numerical calculation of multiphase flows: the Euler–Lagrange approach and the Euler–Euler approach. In the latter approach, different phases are treated as interpenetrating continua and this approach has been widely adopted in ejector modeling. The conservation equations have similar form for all phases in this approach. There are two Euler–Euler multiphase models for ejector modeling: the mixture model and the Eulerian model.

4.2.1. Mixture model

This model solves the momentum, continuity, and energy equations for the mixture while the volume fraction equations are solved only for the dispersed phases. The model uses algebraic expressions for the relative velocities and the equations for multiphase flows are derived by mass-weighted averaging or Favre-averaging method.

The continuity and the momentum equations for mixture flow are,

$$\frac{\partial}{\partial t}(\alpha_{\rm m}\rho_{\rm m}) + \nabla(\alpha_{\rm m}\rho_{\rm m}u_{\rm m}) = \Gamma_{\rm m} \tag{127}$$

$$\frac{\partial}{\partial t}(\rho_{\rm m}u_{\rm m}) + \nabla(\rho_{\rm m}u_{\rm m}u_{\rm m}) = -\nabla P + \nabla(\tau_{\rm m} + \tau T_{\rm m}) + \nabla\tau D_{\rm m} + \rho_{\rm m}g + M_{\rm m} \tag{128}$$

The diffusion stress term $\nabla\tau D_{\rm m}$ represents the momentum diffusion due to the relative motions of the two phases while $M_{\rm m}$ is the influence of the surface tension force on the mixture and depends on the geometry of the interface.

In order to calculate the relative velocity, it is necessary to calculate the average interfacial momentum source for the dispersed phase $M_{\rm p}$. By neglecting the surface tension forces ($M_{\rm m} = 0$) and assuming that the phase pressures are equal and rearranging, the equation for dispersed phase $M_{\rm p}$ is

$$\begin{aligned} M_{\rm p} = {} & \left\{\alpha_{\rm p}(\rho_{\rm p} - \rho_{\rm m})\left[\frac{\partial u_{\rm m}}{\partial t} + (u_{\rm m}\nabla)u_{\rm m} - g\right]\right\} \\ & + \left\{\alpha_{\rm p}\rho_{\rm p}\left[\frac{\partial u_{M_{\rm p}}}{\partial t} + (u_{M_{\rm p}}\nabla)u_{M_{\rm p}}\right]\right\} \\ & + \left\{\alpha_{\rm p}\rho_{\rm p}\left[(u_{\rm m}\nabla)u_{M_{\rm p}} + (u_{M_{\rm p}}\nabla)u_{M_{\rm p}}\right]\right\} \\ & + \left\{-\nabla\left[\alpha_{\rm p}(\tau_{\rm p} + \tau_{T_{\rm p}})\right]\right\} + \alpha_{\rm p}\nabla(\tau_{\rm m} + \tau T_{\rm m} + \tau D_{\rm m}) \end{aligned} \tag{129}$$

The second term from Eq. (128) is omitted by assuming local equilibrium (the bubbles are rapidly accelerated to the terminal rise velocity). The third term corresponds, in rotational motion, to the Coriolis force while the last term is the contributions of the viscous, turbulent and diffusion stresses. These are usually neglected.

By neglecting the virtual mass effect, lift-force effect, basset (or history) effect except the viscous drag and assuming spherical bubbles, the momentum transfer induced by the fluid-fluid interaction force is

$$\begin{aligned} M_{\rm p} &= -\frac{1}{2}\rho_{\rm c}A_{\rm p}C_{\rm D}|u_{\rm cp}|u_{\rm cp} \\ &= -V_{\rm p}(\rho_{\rm p} - \rho_{\rm m})\left[-g + (u_{\rm m}\nabla)u_{\rm m} + \frac{\partial u_{\rm m}}{\partial t}\right] \end{aligned} \tag{130}$$

where $u_{\rm cp}$ is the relative velocity, $u_{\rm cp} = u_{\rm c} - u_{\rm p}$.

Kandakure et al. [37] used the algebraic slip mixture (ASM) model to study the hydrodynamic characteristics of the ejector. The model accounts for the relative velocity between the continuous and dispersed phases as the interfacial momentum exchange term. In the simulation, water was taken as the primary fluid and air as the entrained fluid. The air phase was assumed to obey the ideal gas law. Standard k-ε model was used for modeling the turbulent behavior of the flow. The slip between the phases was taken as some percentage of local primary velocity. They found that at low value of area ratio (ratio of the mixing chamber's throat area to nozzle throat area), due to the larger diameter of the water jet, the annular area available for air flow reduces, causing recirculation of the entrained air within the converging section of the ejector. On the other hand, for higher values of area ratio, due to smaller diameter of the water jet, the momentum transfer to the air decreases and all the entrained air cannot be forced through the throat. As a result, the net air flow rate going into the throat for both area ratios is small. Thus there is an optimum area ratio for the maximum air entrainment rate. The air entrainment rate correlates with pressure difference between the air entry and throat exit for a wide variety of ejector geometries and operating conditions. The overall head loss factor and the ejector efficiency can be predicted a priori.

Kim et al. [38] also investigated the hydrodynamic characteristics of the liquid–gas (water–air) ejectors with mixture model and experiments focusing on the gas hold-up performance. They found the gas phase hold up increases with increasing liquid circulating rate but it decreases with increasing liquid level in the column. The gas suction rate increases with increasing the liquid circulating rate but it decreases with increasing the liquid level in the column and nozzle diameter.

In order to get maximum entrainment of the secondary fluid, Yadav and Patwardhan [39] used the ASM model to determine the optimum geometry of suction chamber of the ejector which is worked as a contactor for two fluids mixing. It is found experimentally that the entrainment of the secondary fluid was more when straight portion of the throat is of zero length [40]. Hence, the geometrical model of the ejector adopted by Yadav and Patwardhan is shown in Fig. 11 with zero length of throat. Also,

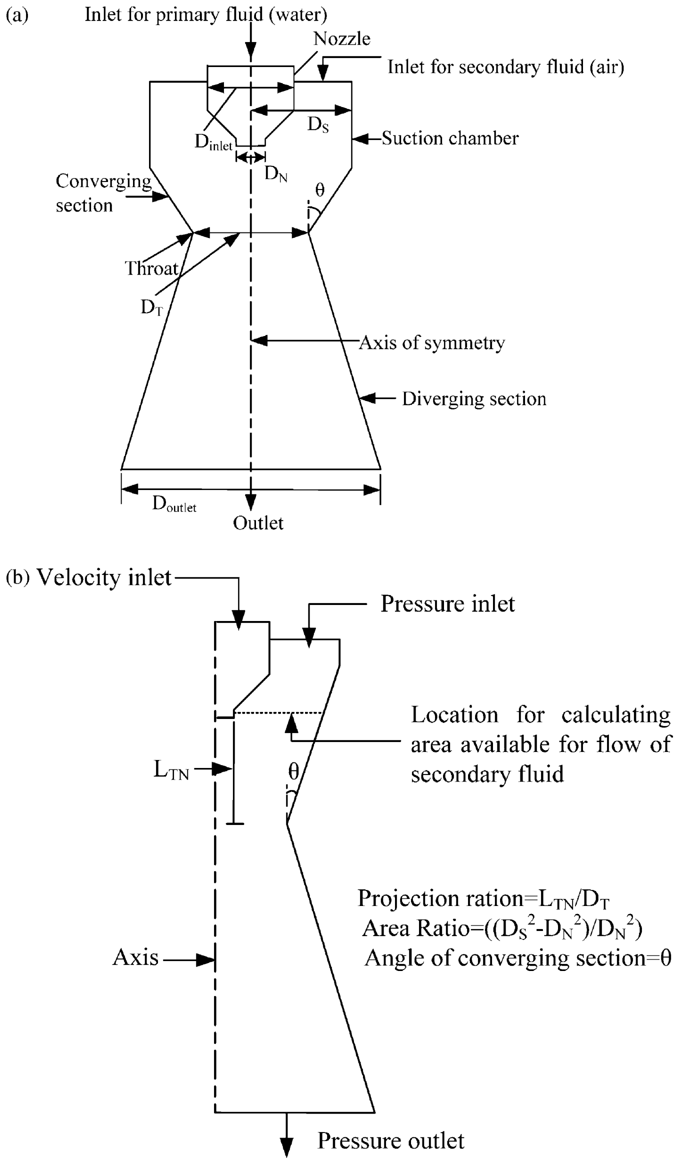


Fig. 11. Geometrical model adopted by Yadav and Patwardhan.

water was taken as the primary fluid and air as the secondary fluid with air assumed to obey the ideal gas law. The standard k-ε turbulence model (per phase) was used to calculate the turbulence. Then they carried out a large number of CFD simulations using the model to understand the effects of the geometrical parameters of the suction chamber on entrainment of the secondary fluid. They found that the geometry of the suction chamber has significant effect on the rate of entrainment of the secondary fluid. After studying the three parameters: the projection ratio (PR: distance between nozzle tip and entry to throat), area ratio and angle of the converging section based on the model, Yadav and Patwardhan recommended that a PR of five produces the highest rate of entrainment of the secondary fluid. Increasing the PR beyond five does not lead to any significant improvement in the suction capacity of the jet. In addition, they found a suction chamber with $(D_s^2 - D_n^2)/D_n^2 = 6.6$ (D_s: diameter of suction chamber, D_n: diameter of nozzle exit) gives the largest entrainment. A larger suction chamber leads to a reduction in suction capacity. The angle of converging section is recommended in the range of 5°–15°.

The previously mentioned models are taken water as primary fluid and air as secondary fluid. Balamurugan et al. [41] used the mixture model with standard k-ε turbulence model to investigate the hydrodynamic characteristics of ejectors using air as the primary fluid and water as the entrained fluid. Both air and water were considered at room temperature. The air was assumed to obey an ideal gas law. They observed that the liquid entrainment rate increases with an increase in the liquid level and the gas velocity. The entrainment rate was found to be the highest corresponding to area ratio of about 0.155.

4.2.2. Eulerian model

The Eulerian model solves the momentum and continuity equations for each phase separately. The coupling of the equations is achieved through the pressure and inter-phase exchange coefficients. Momentum exchange between the phases is also dependent upon the type of mixture under consideration.

The continuity equation and the momentum equations for the Eulerian model are the same as the mixture model. The average interfacial momentum source for the phase k is

$$M_k = \sum_{j=1}^{n}(R_{jk} + m_{jk}u_{jk}) + \alpha_k\rho_k(F_k + F_{\mathrm{lift},k} + F_{vm,k}) \tag{131}$$

where F_k is an external body force, $F_{\mathrm{lift},k}$ is a lift force, $F_{vm,k}$ is a virtual mass force, R_{jk} is an interaction force between phase i and phase k and p is the pressure shared by all the phases. The lift force acts on a dispersed phase due to velocity gradient in the continuous-phase flow field, is:

$$F_{\mathrm{lift,p}} = -0.5\rho_c\alpha_p(u_c - u_p) \times (\nabla \times u_c) \tag{132}$$

For multiphase flows, the virtual mass effect occurs when a dispersed phase accelerates relative to the continuous phase. The inertia of the continuous phase mass encountered while accelerating dispersed phase exerts a "virtual mass force" on the dispersed phase, which is given by:

$$F_{vm,p} = 0.5\alpha_p\rho_c\left(\frac{D}{Dt}(u_c - u_p)\right) \tag{133}$$

Eulerian model assumes dispersion type flow where the secondary fluid is distributed in the primary fluid. However, in Yadav and Patwardhan's [39] work, the ejector was arranged such that the water jet was directed downwards. The entrained air flowed around the water jet in the annular space between the water jet and the ejector. They found no bubble formation inside the ejector and both the fluids flowed co-currently. Since there was no bubble, the virtual mass, which arises from acceleration, and lift force, which arises from unbalanced pressure forces around the bubble, do not exist. Hence, the Eulerian model is not a suitable choice for studying the coaxial type of flows in ejector.

The previously mentioned models consider the primary and secondary fluids are of different chemical compositions with non-condensable gas. However, when both fluids are of the same chemical composition, the vapor is condensable in the fluid, there may be need a different model to simulate the hydrodynamic performance of the ejector. Therefore, Narabayashi et al. [42] derived a separate two-phase flow model to analysis the performance of a steam injector entrained by high pressure water in order to check the feasibility of a large-scale steam injector for which a demonstration test was not able to be conducted. In the model, attention was paid on the radial heat transport enhancement by the turbulence because of relatively large-scale water jet being used. Also, the interface activation was taken into account. The model including steam phase, water phase and the interface is shown as follows.

Steam:

$$\mathrm{div}(\rho_g \vec{U}_g) = -m_{gl} \tag{134}$$

$$\mathrm{div}(\rho_g \vec{U}_g V_g - \Gamma \upsilon_g \mathrm{grad} V_g) = -\frac{\partial P}{\partial r} \tag{135}$$

$$\mathrm{div}(\rho_g \vec{U}_g W_g - \Gamma \upsilon_g \mathrm{grad} W_g) = -\frac{\partial P}{\partial z} + C_i |W_g - W_i|(W_g - W_i) \tag{136}$$

$$\mathrm{div}(\rho_g \vec{U}_g h_g - \Gamma h_g \mathrm{grad} h_g) = -\frac{DP}{DT} + \Phi \tag{137}$$

$$div(\rho_g \vec{U}_g k_g - \Gamma k_g \mathrm{grad} k_g) = G k_g - \rho_g \varepsilon_g \tag{138}$$

$$\mathrm{div}(\rho_g \vec{U}_g \varepsilon_g - \Gamma \varepsilon_g \mathrm{grad}\, \varepsilon_g) = C_1 \frac{\varepsilon_g}{k_g} G k_g - C_2 \rho_g \varepsilon_g^2 / k_g \tag{139}$$

Water

$$\mathrm{div}(\rho_l \vec{U}_l) = -m_{gl} \tag{140}$$

$$\mathrm{div}(\rho_l \vec{U}_l V_l - \Gamma \upsilon_l \mathrm{grad} V_l) = -\frac{\partial P}{\partial r} \tag{141}$$

$$\mathrm{div}(\rho_l \vec{U}_l W_l - \Gamma \upsilon_l \mathrm{grad} W_l) = -\frac{\partial P}{\partial z} + C_i |W_g - W_i|(W_g - W_i) + m_{gl} W_g \tag{142}$$

$$\mathrm{div}(\rho_l \vec{U}_l h_l - \Gamma h_l \mathrm{grad} h_l) = 0 \tag{143}$$

$$\mathrm{div}(\rho_l \vec{U}_l k_l - \Gamma k_l \mathrm{grad} k_l) = G k_l - \rho_l \varepsilon_l \tag{144}$$

$$\mathrm{div}(\rho_l \vec{U}_l \varepsilon_l - \Gamma \varepsilon_l \mathrm{grad}\, \varepsilon_l) = C_1 \frac{\varepsilon_g}{k_l} G k_l - C_2 \rho_l \varepsilon_l^2 / k_l \tag{145}$$

4.2.3. Interface

Assuming direct condensation onto the surface of the water jet, the heat transfer coefficients of direct condensation are given for each interface cell surface, by using the ideal condensation based on the Clausius–Clapeyron equation and Bernoulli's theorem:

$$H_{ci} = \sqrt{2} h_{lg}^{3/2} / ((\upsilon_g(\upsilon_g - \upsilon_l))(T_{sat}(T_{sat} - T_{li})))^{1/2} \tag{146}$$

$$m_{gl} = H_{ci}(T_s - T_{li}) A_i / h_{lg} \tag{147}$$

$$\mathrm{div}(\rho_l \vec{U}_l h_l - \Gamma h_l \mathrm{grad} h_l) = m_{gl} h_g \tag{148}$$

The interface velocities between the phases for each interface cell surface are:

$$W_{li} = (\tau_g W_g + \tau_l W_l)/(\tau_g + \tau_l) \tag{149}$$

where τ_g is the gas shear stress and τ_l is the liquid shear stress, C_i is the shear coefficient of interface between gas and liquid phases and the subscript and i is interface between gas and liquid phases.

They verified the model by using high pressure steam test data (high pressure small size model), as well as the visualized data such as temperature and pressure distribution data. Good agreements were found between the test results and the analysis results. Then they used the model to analysis the characteristics of the large-scale steam injector which shown that the steam injector driven jet pump could work in the high pressure range over 7 MPa, and discharged over 12 MPa even at the large-scale rated flow rate of 220 ton per hour.

5. Empirical/semi-empirical model

The physical phenomena involve supersonic flow, shock interactions, and turbulent mixing of two streams inside the ejector enclosure which are difficult to be modeled precisely. Also, the solving process of the models based on the physical phenomena is complicated and time-consuming. Hence, in order to the evaluate the ejector performance and to instruct design, Huang et al. [43] derived empirical correlations for ejector design using R141b as the working fluid after experimented on 15 sets of ejectors:

$$\frac{A_e}{A_{nt}} = -0.0517\left(\frac{A_m}{A_{nt}}\right)^2 + 1.4362\left(\frac{A_m}{A_{nt}}\right) - 4.1734 \tag{150}$$

$$\frac{A_m}{A_{nt}} = b_0 + b_1 r_c + b_2 r_c{}^2 + b_3 r_g + b_4 r_c r_g + b_5 r_c{}^2 r_g + b_6 r_g{}^2 + b_7 r_c r_g{}^2 + b_8 r_c{}^2 r_g{}^2 \tag{151}$$

where $r_c = P_c^*/Pe; r_g = P_1/P_e$ and the $b_0 \sim b_8$ are coefficients.

Cizungu et al. [21] worked out following correlation based on the experimental investigations of Dorantès and Lallemand [44] to estimate the entrainment ratio of the ejector:

$$\omega = 3.32\left(\frac{1}{\psi} - \frac{1.21}{\xi\psi}\right)^{2.12} \tag{152}$$

where $2.5 \leq \xi \leq 4$, $\psi \leq 6$.

However, the empirical model cannot be extent to other fluid and ejector. In order to derive a relationship working for more fluids and physical configurations, Chou et al. [45] regressed a relationship for the maximum flow ratio against the geometry based on the experimental results from literatures [9,12,46–48]:

$$\frac{m_s}{m_p} = \left(\frac{P_e}{P_g}\right)\frac{1}{(T_e/T_g)^{1/2}} K_p K_f K_s \varphi \tag{153}$$

where K_p accounts for the primary nozzle performance,

$$K_p = -\left(\frac{P_e}{P_g}\right)^2 + \lambda F P_\delta \left(\frac{P_e}{P_g}\right) \tag{154}$$

wherein λ is the correction constant for the primary nozzle working range and FP_δ is the failure pressure ratio of the primary nozzle. K_f is the physical effective area ratio proposed by Solokov and Zinger [49], $K_f = \mu \times ff - \frac{A_{pp}}{A_t}$, where $ff = \frac{A_3}{A_t}$ is the ejector geometric design area ratio for the ejector, A_{pp} is the area of primary flow at choking location and μ is a correction constant of between 1.35 and 1.5; K_s accounts for the "blockage effect" of the ejector configuration, affecting the entrainment and mixing process and φ is an application specific correction factor which can be applied to an ejector operating with a given refrigerant and system configuration. $K_s = (L_s/\Delta)^{b-M}$, where L_s/Δ is the flow aspect ratio (L_s is the length of the suction chamber, i.e. convergent section of mixture) and Δ is the radius of A_3); b is the Mach number limitation constant, 4 for R113 and R141b and 5.2 for steam, and M is the design exit Mach number of the primary nozzle.

More investigators have performed detailed experiments and developed numerous empirical correlations to predict the entrainment ratio, gas hold-up, mass transfer coefficient and interfacial area based on the flow direction: vertical up-flow, vertical down-flow and horizontal flow. Balamurugan et al. [50] summarized in detail of these correlations which will not be covered here. As most of the models are based on liquid as the primary fluid and gas as the entrained fluid, Balamurugan et al. [50] developed a semi-empirical model to predict the liquid entrainment rate (gaseous as primary fluid) taking into account: the compressible nature of

air in the nozzle, pressure drop for two-phase flow and the losses due to change in cross sectional area.

The entrainment ratio : ω

$$= -7.51\left(\frac{P_p}{P_s}\right)^2 + 9.93\left(\frac{P_p}{P_s}\right) - 2.31 \quad (155)$$

The previously mentioned empirical or semi-empirical models are regressed from measurements. They are limited to the range over which it was developed, which limits their use in investigating the performance of new ejector fluids, designs or operating conditions. Hence, Dessouky et al. [5] developed a semi-empirical model based on the basic model similar as [10] and a large database extracted from several ejector manufacturers and a number of experimental literature studies with attempting to eliminate the need for iterative procedures and simple to use, also give more flexibility in ejector design and performance evaluation comparing with empirical model.

The correlations for steam ejector performance evaluation are:

$$\omega = aEr^b P_e{}^c P_c{}^d \frac{(e + fP_p{}^g)}{(h + iP_c{}^j)} \quad (156)$$

$$\omega = aEr^b P_e{}^c P_c{}^d \frac{(e + f\ln(P_p))}{(g + h\ln(P_c))} \quad (157)$$

wherein, *a*–*i* are the coefficients. The former is used for the entrainment ratio of choked flow or compression ratios above 1.8 while the latter is used for the entrainment ratio of un-choked flow with compression ratios below 1.8. They also worked out correlations used for design:

For choked flow:

$$P_{np} = 0.13P_s^{0.33}P_c^{0.73} \quad (158)$$

$$A_{nt}/A_m = 0.34P_c^{1.09}P_p^{-1.12}\omega^{-0.16} \quad (159)$$

$$A_{np}/A_{nt} = 1.04P_c^{-0.83}P_p^{0.86}\omega^{-0.12} \quad (160)$$

For un-choked flow:

$$P_{np} = 1.02P_s^{-0.000762}P_c^{0.99} \quad (161)$$

$$A_{nt}/A_m = 0.32P_c^{1.1}P_p^{-1.13}\omega^{-0.36} \quad (162)$$

$$A_{np}/A_{nt} = 1.22P_c^{-0.81}P_p^{0.81}\omega^{-0.0739} \quad (163)$$

They compared the results of the semi-empirical model with the experimental results derived from other literatures [6,9,48,51–55] and good agreements were found.

Besides, they derived an empirical model for ejector performance analysis [56] based on the data and method presented by Power [11]:

$$\omega = 0.296\frac{(P_{exit})^{1.19}}{(P_s)^{1.04}}\left(\frac{P_p}{P_s}\right)^{0.015}\left(\frac{PCF}{TCF}\right) \quad (164)$$

PCF is the primary steam pressure correction factor and TCF is the entrained vapor temperature correction factor. They are defined as:

$$PCF = 3 \times 10^{-7}(P_p)^2 - 0.0009(P_p) + 1.6101 \quad (165)$$

$$TCF = 2 \times 10 - 8(T_s)^2 - 0.0006T_s + 1.0047 \quad (166)$$

The model equations are valid only for an ejector operating with steam as the primary fluid and the entrained fluid is water vapor. These equations are valid over the following ranges: $4500 \geq T_s > 10\,^\circ C$, $3500 \geq P_p \geq 100$ kPa, and $P_{exit}/P_s \geq 1.81$.

6. Conclusion

Various mathematical models have been proposed to assess the performance of ejector for different operation and design conditions. Generally, the mathematical models are based on the flow and mixing phenomena inside the system. They can be divided into two main categories in terms of thermodynamic model and dynamic model. Within the two categories, the models can be subdivided based on flowing phases. Both thermodynamic model and dynamic model have two types: single-phase flow and two-phase flow. The single-phase flow thermodynamic model can be classified into two sub-categories according to the mixing mechanism: constant-pressure mixing model and constant-area mixing model. The two-phase dynamic model can be further subdivided based on the calculation methods: mixture model and Eulerian model. Also, using the measurements data, several empirical/semi-empirical models to evaluate the performance of ejector and to guide ejector design are reviewed in this paper.

Thermodynamic models are usually expressed in explicit algebraic equations and are based on the steady-state one-dimensional model, focused on the pressure change caused by supersonic shock. In these models, the detailed local interactions between shock waves and boundary layers, their influence on mixing and recompression rate are not taken into account. Lumped method is applied in the governing equations which lead to simple model with lower accuracy. In order to offer good accuracy in predicting the performance of the ejector by the thermodynamic model, some isentropic coefficients accounting for the friction loss were applied in the model and were determined by experiment. In these models, certain knowledge on the choking, shock and mixing should be obtained in advance and assumptions should be made for model simplification. The more practical models known as constant-pressure mixing model and constant-area mixing model made the model feasible. The constant-pressure mixing ejector provides better performance than the constant-area mixing ejector. While the constant-area mixing model gives more accurate performance prediction. In order to give more accurate prediction, the two-phase flowing model is developed considering the condensation of the secondary flow or the mixture of two streams in different phase states. In these models, quality is introduced in the calculation of the state parameters. Though the governing equations are basically the same as single-phase flowing model, the accuracy is improved.

The dynamic model, on the contrary, accounts the turbulence interaction between the primary and secondary stream, the shock reflection and chocking. It is more related to the actual process occurred in the ejector and the effect of the geometrical parameters and operation parameters can be well explained. The precision of this model is thus greatly improved.

The flow in the ejector is from supersonic to sonic, and then to subsonic. Therefore, the choice of the turbulence model is important. For compressible flowing model, it was found RNG *k*-ε and *k*-ω-SST models were the best suited to predict the shock phase, strength, and the mean line of pressure recovery [31]. For incompressible flow, the standard *k*-ε model and realizable *k*-ε model were widely used for time saving. For two-phase flowing model, the mixture model can give reasonable results.

It can be seen that the pressure inlet and pressure outlet boundary conditions are widely used in all the models whenever possible. Other boundary conditions such as mass flow rate or velocity are seldom used in models. For thermodynamic model, the auxiliary relations such as gas dynamic equations, the defining of

Mach number and sonic velocity, the state expression have to be employed to complete the mathematical model.

Due to the complex nature of the partial differential equations, it is necessary to solve the mathematical model using numerical methods. Finite difference method is recognized as the most accurate and most universal solution technique and is widely employed in ejector modeling.

Besides, model validation is an important step in model development since it offers the possibility of comparing simulation results with actual system behavior. Experiments are mostly used to validate the mathematical model. Besides, comparing with the previous numerical results is also a good validation method.

Though a large amount of works have been conducted on modeling and analyzing ejector, further efforts are still needed:

(1) To study the influence of variable isentropic coefficients which are taken as constant in almost all existing thermodynamic models.
(2) To improve the accuracy of the model based on turbulence model, since by now, there still no uniform model being used.
(3) To construct a simulation package of the whole ejector-based system by combining the model of the ejector and other components in the system.

Acknowledgements

It is gratefully acknowledged that financial support for this work has been provided by the Key Project of the Natural Science Foundation of China under the contract No. 50736004.

References

[1] Paul J, Jahn E. Water as refrigerant. 19th International Congress of Refrigeration, Proceedings IVb. August 20–25, 1995:955–974.
[2] Chunnanond K, Aphornratana S. Ejectors: applications in refrigeration technology. Renewable Sustainable Energy Reviews 2004;8(2):129–55.
[3] Zhang B, Shen S. Development of solar ejector refrigeration system. 1st International Conference on Sustainable Energy Technologies. 2002.
[4] Sun DW, Eames IW. Recent developments in the design theories and applications of ejectors—a review. Journal of Institute Energy 1995;68:65–79.
[5] El-Dessouky H, Ettouney H, Alatiqi I, Al-Nuwaibit G. Evaluation of steam jet ejectors. Chemical Engineering and Processing 2002; 41:551–561.
[6] Munday JT, Bagster DF. A new theory applied to steam jet refrigeration. Industrial & Engineering Chemistry Process Design and Development 1977;16:442–9.
[7] Keenan JH, Neumann EP, Lustwerk F. An investigation of ejector design by analysis and experiment. ASME Journal of Applied Mechanics 1950;72:299–309.
[8] Keenan JH, Neumann EP. A simple air ejector. ASME Journal of Applied Mechanics 1942;64:75–82.
[9] Eames IW, Aphornratana S, Haider H. A theoretical and experimental study of a small-scale steam jet refrigerator. International Journal of Refrigeration 1995;18(6):378–86.
[10] Aly NH, Aly K., Shamloul MM. Modelling and simulation of steam jet ejectors. Desalination 1999; 123:1–8.
[11] Power BR. Steam jet ejectors for process industries. New York: McGraw Hill; 1994.
[12] Huang BJ, Chang JM, Wang CP, Petrenko VA. A 1D analysis of ejector performance. International Journal of Refrigeration 1999;22:354–64.
[13] Rogdakis ED, Alexis LK. Design and parametric investigation of an ejector in an air-conditioning system. Applied Thermal Engineering 2000;20(2):213–26.
[14] Selvaraju A, Mani A. Analysis of an ejector with environment friendly refrigerants. Applied Thermal Engineering 2004;24(5–6):827–38.
[15] Yu J, Ren YF, Chen H, Li YZ. Applying mechanical subcooling to ejector refrigeration cycle for improving the coefficient of performance. Energy Conversion and Management 2007;48:1193–9.
[16] Ouzzane M, Aidoun Z. Model development and numerical procedure for detailed ejector analysis and design. Applied Thermal Engineering 2003;23(18):2337–51.
[17] Grazzini G, Mariani A. A simple program to design a multi-stage jet-pump for refrigeration cycles. Energy Conversion and Management 1998; 39(16–18):1827–1834.
[18] Yapici R, Ersoy HK. Performance characteristics of the ejector refrigeration system based on the constant area ejector flow model. Energy Conversion and Management 2005;46:3117–35.
[19] Sun DW, Eames IW. Performance characteristics of HCFC-123 ejector refrigeration cycles. International Journal of Energy Research 1996;20:871–85.
[20] Sherif SA, Lear WE, Steadham JM, Hunt PL, Holladay JB. Analysis and modeling of a two-phase jet pump of a thermal management system for aerospace applications. International Journal of Mechanical Sciences 2000;42(2):185–98.
[21] Cizungu K, Lroll M, Ling ZL. Modelling and optimization of two-phase ejectors for cooling systems. Applied Thermal Engineering 2005;25(13):1979–94.
[22] Beithou N, Aybar HS. A mathematical model for steam-driven jet pump. International Journal of Multiphase Flow 2000;26(10):1609–19.
[23] Cattadori L, Lalbiati L, Vanini P. A single-stale high pressure steam injector for next-generation reactors: test result and analysis. International Journal Multiphase Flow 1995;21:591–606.
[24] Deberne N, Leone JF, Duque A, Lallemand A. A model for calculation of steam injector performance. International Journal of Multiphase Flow 1999;25(5):841–55.
[25] Young JB, Guha A. Normal shock-wave structure in two-phase vapour-droplet flows. Journal of Fluid Mechanics 1991;228:243–74.
[26] Smith SJ, Riffat SB, Wu S, Eames IW. Low-pressure ejectors: prediction of performance by computational fluid dynamics. Building Services Engineering and Research Technology 1997;18(3):179–82.
[27] Riffat SB, Everitt P. Experimental and CFD modelling of an ejector system for vehicle air conditioning. Journal of Institute of Energy 1999;72:41–7.
[28] Riffat SB, Omer SA. CFD modelling and experimental investigation of an ejector refrigeration system using methanol as the working fluid. International Journal of Engineering Research 2001;25:115–28.
[29] Rusly E, Lu Aye, Charters WWS, Ooi A. CFD analysis of ejector in a combined ejector cooling system. International Journal of Refrigeration 2005;28:1092–101.
[30] Bartosiewicz Y, Aidoun Z, Desevaux P, and Mercadier Y. CFD-experiments integration in the evaluation of six turbulence models for supersonic ejectors modeling. Conference Proceedings, Integrating CFD and Experiments, Glasgow, UK. 2003.
[31] Bartosiewicz Y, Aidoun Z, Desevaux P, Mercadier Y. Numerical and experimental investigations on supersonic ejectors. International Journal of Heat and Fluid Flow 2005;26:56–70.
[32] Desevaux P, Aeschbacher O. Numerical and experimental flow visualization of the mixing process inside an induced air ejector. International Journal of Turbo Jet Engines 2002;19:71–8.
[33] Desevaux P, Lanzetta F, Bailly Y. CFD modelling of shock train inside a supersonic ejector: validation against flow visualization and pressure measurements in the case of zero-secondary flow. Conference Proceedings, 10th International Symposium on Flow Visualization, Kyoto, Japan. 2002.
[34] Bartosiewicz Y, Aidoun Z, Mercadier Y. Numerical assessment of ejector operation for refrigeration applications based on CFD. Applied Thermal Engineering 2006;26:604–12.
[35] Zhu YH, Cai WJ, Wen CY, Li YZ. Numerical investigation of geometry parameters for design of high performance ejectors. Applied Thermal Engineering (in press).
[36] Pianthong K, Seehanam W, Behnia M, Sriveerakul T, Aphornratana S. Investigation and improvement of ejector refrigeration system using computational fluid dynamics technique. Energy Conversion and Management 2007;48:2556–64.
[37] Kandakure MT, Gaikar VG, Patwardhan AW. Hydrodynamic aspects of ejectors. Chemical Engineering Science 2005;60:6391–402.
[38] Kim MI, Kim OS, Lee DH, Kim SD. Numerical and experimental investigations of gas–liquid dispersion in an ejector. Chemical Engineering Science 2007;62:7133–7139.
[39] Yadav RL, Patwardhan AW. Design aspects of ejectors: effects of suction chamber geometry. Chemical Engineering Science 2008;63(15):3886–97.
[40] Bhutada SR, angarkar VG. Gas induction and hold-up characteristics of liquid jet loop reactors. Chemical Engineering communications 1987;61:239–61.
[41] Balamurugan S, Gaikar VG, Patwardhan AW. Effect of ejector configuration on hydrodynamic characteristics of gas-liquid ejectors. Chemical Engineering Science 2008;63:721–31.
[42] Narabayashi T, Mizumachi W, Mori M. Study on two-phase flow dynamics in steam injectors. Nuclear Engineering and Design 1997;175:147–156.
[43] Huang BJ, Chang JM. Empirical correlation for ejector design. International Journal of Refrigeration 1999;22(5):379–88.
[44] Dorantès R, Lallemand A. Prediction of performance of a jet cooling system operating with pure refrigerants or non-azeotropic mixtures. International Journal of Refrigeration 1995;18(1):21–30.
[45] Chou SK, Yang PR, Yan C. Maximum mass flow ratio due to secondary flow choking in an ejector refrigeration system. International Journal of Refrigeration 2001;24:486–99.
[46] Huang BJ, Jiang CB, Hu FL. Ejector performance characteristics and design analysis of jet refrigeration system. ASME Journal of Engineering for Gas Turbines and Power 1985;107:792–802.
[47] Huang M-C, Chen S-L, An experimental investigation of ejector performance characteristics in a jet refrigeration system, Journal of the Chinese Institute of Chemical Engineers 1996, 27(2):91–100.
[48] Chen YM, Sun CY. Experimental study of the performance characteristics of a steam-ejector refrigeration system. Experimental Thermal and Fluid Science 1997;(15):384–94.

[49] Solokov ER, Zinger NM. Jet devices, Energiya, Moscow, 1970 (in Russian).
[50] Balamurugan S, Lad MD, Gaikar VG, Patwardhan AW. Hydrodynamics and mass transfer characteristics of gas–liquid ejectors. Chemical Engineering Journal 2007;131(1–3):83–103.
[51] Aphornratana S, Eames IW. A small capacity steam-ejector refrigerator: experimental investigation of a system using ejector with movable primary nozzle. International Journal of Refrigeratrion 1997;20:352–8.
[52] Bagster DF, Bresnahan JD. An examination of the two-stream theory of steam-jet ejectors. Proceedings of the 11th Australian Conference on Chemical Engineering. Brisbane. 1983.
[53] Sun DW. Variable geometry ejectors and their applications in ejector refrigeration system. Energy Conversion 1996;21:919–29.
[54] Arnold HG, Huntley WR, Perez-Blanco H. Steam ejector as an industrial heat pump. ASHRAE Transactions 1982;88:845–57.
[55] Everitt P, Riffat SB. Steam jet ejector for vehicle air conditioning. International Journal of Ambient Energy 1999;20:14–20.
[56] El-Dessouky H, Ettouney H, Al-Fulaij H, Mandani F. Multistage flash desalination combined with thermal vapor compression. Chemical Engineering and Processing 2000; 39: 343-356.